Efficient structural relaxation based on the random phase approximation: Applications to the water clusters

Muhammad N. Tahir,[†] Honghui Shang,[*,‡] Jia Li,[*,¶] and Xinguo Ren[*,†]

†*Institute of Physics, Chinese Academy of Sciences, Beijing 100190, China*

‡*University of Science and Technology of China, Hefei 230026, China*

¶*Shenzhen Geim Graphene Center and Institute of Materials Research, Tsinghua Shenzhen International Graduate School, Tsinghua University, Shenzhen 518055, China*

E-mail: shh@ustc.edu.cn; li.jia@sz.tsinghua.edu.cn; renxg@iphy.ac.cn

Abstract

We report an improved implementation for evaluating the analytical gradients of the random phase approximation (RPA) electron-correlation energy based on atomic orbitals and the localized resolution of identity scheme. The more efficient RPA force calculations allow us to relax structures of medium-size water clusters. Particular attention is paid to the structures and energy orderings of the low-energy isomers of $(H_2O)_n$ clusters with $n = 21$, 22, and 25. It is found that the energy ordering of the low-energy isomers of these water clusters are rather sensitive to how their structures are determined. For the five low-energy isomers of $(H_2O)_{25}$, the RPA energy ordering based on the RPA geometries is quite different from that based on the geometries relaxed by lower-level theories, in contrast with the situation of small water clusters like the water hexamer. The standard RPA underbinds the water clusters, and this underbinding behavior gets more pronounced as the complete basis set (CBS) limit is approached. The renormalized single excitation (rSE) correction remedies this underbinding, giving rise to a noticeable overbinding behavior at finite basis sets. However, as the CBS limit is approached, RPA+rSE yields an accuracy for the binding energies that is comparable to the best available double hybrid functionals, as demonstrated for the WATER27 testset.

1 Introduction

Water clusters $(H_2O)_n$ are the building blocks of bulk water – the most important substance for life on earth. Studying the structures and properties of water clusters is a crucial step towards a molecular-level understanding of water in its condensed phases, including both liquid water and ice.[1,2] Moreover, water clusters themselves are important components of biological systems and are abundant in atmosphere, and hence studying the properties of water clusters is of high scientific interest by its own. Experimental and computational studies of water clusters have been continued for decades, yet numerous questions remain to be addressed,

in particular regarding the energy rankings of low-lying isomers at each cluster size.[3] The commonly used computational approaches for these studies range from classical force fields to density functional approximations (DFAs) and *ab initio* quantum chemistry methods. Due to the rapid increase in the numbers of local minimum structures of $(H_2O)_n$ as the size n grows, global structure search has mainly been carried out based on classical force fields, generated either empirically[4] or fitted to *ab initio* data.[5,6] The initially determined structures and their energies can then be refined using more accurate first-principles methods.[3] In the quest for fully understanding the properties of water clusters (and ultimately bulk water), it is crucial to have inexpensive yet sufficiently accurate quantum chemical methods that can treat electrostatics, hydrogen bonding and van der Walls (vdW) interactions on an equal footing. In this regard, the second-order Møller-Plesset perturbation theory (MP2),[7] simplest post-Hartree-Fock quantum-chemistry method, plays a pivotal role in the study of water clusters as it often delivers highly reliable results, and is often used to benchmark the accuracy of DFAs.[8,9]

In recent years, the random phase approximation (RPA),[10–14] formulated as an orbital-dependent fifth-rung functional of density functional theory (DFT),[15–17] has emerged as a powerful first-principles approach to evaluate the electronic ground-state energies of molecules and extended materials. Compared to lower-rung functionals, one prominent advantage of RPA is that it captures seamlessly the long-range van der Waals (vdW) interactions.[18,19] Benchmark calculations showed that RPA-based methods can accurately describe the interactions within weakly bonded molecular complexes[20–25] and are capable of capturing the delicate energy differences between different structural configurations[26,27] and crystalline polymorphs.[28–32] Furthermore, compared to MP2, RPA can describe the polarization effects beyond the second order[33] and is applicable to small-gap and metallic systems. As such, there is a strong interest in applying RPA-based methods to water systems. Preliminary results on water clusters,[34,35] liquid water,[36,37] and ices[38] show the great promise of RPA-based methods in characterizing small energy differences in water systems. Given such initial

successes, it is natural to think of determining the structures of water clusters based on the PRA methods. Previously, MP2 is often employed as the high-level benchmark *ab-initio* approach to determine the structures of water clusters.[3,9] In this regard, one expects that RPA may provide a competitive alternative.

To determine the molecular structures at the RPA level, the analytical gradients of the RPA energy with respect to the atomic displacements need to be evaluated. Within the last decade, much effort has been devoted to implementing the analytical gradients of RPA, mostly for molecular geometries. Among these, Rekkedal *et al.*[39] were the first to develop an $\mathcal{O}(N^6)$-scaling algorithm for evaluating the analytical gradient of RPA on top of the Hartree-Fock (HF) reference, utilizing the ring-coupled-cluster-doubles (rCCD) formulation of RPA. Shortly after, a similar rCCD-based analytical gradient formalism for RPA was developed by Mussard *et al.*[40] within the range-separation framework. Based on the resolution of identity (RI) technique and Lagrangian formalism, Burow *et al.*[41] reduced the scaling behavior of RPA gradient calculations to $\mathcal{O}(N^4\log(N))$, taking the size dependence of the imaginary frequency grid into account. Further development was carried out by Ramberger *et al.*[42] who achieved an $\mathcal{O}(N^3)$-scaling RPA gradient algorithm for periodic systems based on the Green's function formalism and plane-wave basis set. The $\mathcal{O}(N^3)$ scaling was enabled by the space-time algorithm for evaluating the GW self-energy,[43,44] which is needed in this particular RPA gradient formalism.[42] This algorithm was further reduced to $\mathcal{O}(N^2)$ by Beuerle *et al.*[45] in terms of an atomic-orbital (AO) formulation whereby the sparsity of the AO-based integrals can be exploited. Recently, the present authors also developed a RPA gradient approach[35] for molecular calculations within the localized RI (LRI) scheme,[46] which works for both Gaussian-type orbital (GTO) and numerical atomic orbital (NAO) basis sets. In the present work, we further improve our algorithm and code, achieving a *de facto* $\mathcal{O}(N^3)$-scaling for RPA gradient calculations. This enables the structure relaxation of molecules of much bigger size at the RPA level, especially for water clusters of medium size ($n > 20$).

RPA has been previously used to study small water clusters. An earlier study of water

clusters using RPA in a dual hybrid form (the so-called dRPA75 functional[47]) was carried out by Mezei *et al.*[48] Using the standard RPA, Chedid *et al.* performed a systematic study of the WATER27[49] testset, benchmarking the performance of RPA for the structural, energetic, and vibrational properties of this testset. They particularly studied the basis set dependence of the RPA binding energies. In consistent with previous experience, they found a substantial underbinding and pronounced basis set dependence of RPA for water clusters. However, despite its overall underbinding behavior, RPA does yield the correct energy ordering for the low-lying isomers of water hexamers.[34,50] Previously, it was found that the underbinding behavior of RPA can be largely cured by adding the renormalized single excitation (rSE) corrections,[25,51] and the efficacy of rSE was also observed in water-cluster systems.[35,52] Thus, we expect that adding rSE corrections to RPA is essential for the RPA-based methods to describe the water systems quantitatively.

In this work, after recapitulating the basic algorithm of our implementation, we present a performance study of our RPA gradient implementation, thereby checking its scaling behavior, parallel efficiency, and numerical accuracy. Then we look at the energy hierarchy of the low-lying isomers of water clusters of larger size, with n = 21, 22, and 25. In particular, we check how the energy ordering of different water isomers change with the level of theories employed to relax their structures. We found that, unlike the water hexamers where going from PBE to RPA geometries the energy ordering is preserved, for larger clusters like $(H_2O)_{25}$, this is not the case any more. If one trusts that RPA-based methods yield reliable energy hierarchy of water clusters, it seems that, in general, it is also important to determine the geometries consistently at the RPA level. We then also checked the basis set convergence for both RPA and RPA+rSE. It is found that as one increases the basis size towards the complete basis set (CBS) limit, the RPA becomes even more underbinding for water clusters, in consistent with Ref. 34, whereas the RPA+rSE evolves from an overbinding behavior towards an excellent agreement with the most accurate results yielded by double hybrid functionals, reported in the literature. Hopefully the present study will shed new

light on the application of RPA-based methods to the study of water systems.

2 Theory and Algorithm

2.1 RPA total energy within the LRI approximation

We start with the RPA total-energy expression and then consider its derivatives with respect to the atomic displacements, highlighting the reduction of the computational cost brought about by the localized RI (LRI). The RPA total energy is given by

$$E^{\mathrm{RPA}} = E^{\mathrm{HF}} + E_c^{\mathrm{RPA}} \tag{1}$$

where E^{HF} is the Hartree-Fock total energy evaluated using orbitals generated from a preceding calculation based on density functional approximations (DFAs). The Perdew-Burke-Ernzerhof (PBE) generalized gradient approximation (GGA) is often used to generate the orbitals and orbital energies for RPA calculations. The key component in Eq. (1), the RPA correlation energy, is formally given by

$$E_c^{\mathrm{RPA}} = \frac{1}{2\pi}\int_0^\infty d\omega \mathrm{Tr}\Big[\ln\big(1-\chi^0(i\omega)v\big) + \chi^0(i\omega)v\Big] \tag{2}$$

where χ^0 is non-interacting Kohn-Sham (KS) response function, which has an explicit "sum-over-states" expression,

$$\chi^0(\mathbf{r},\mathbf{r}',i\omega) = \sum_m \sum_n \frac{(f_m - f_n)\psi_m(\mathbf{r})\psi_n(\mathbf{r})\psi_n(\mathbf{r}')\psi_m(\mathbf{r}')}{\epsilon_m - \epsilon_n - i\omega}\,, \tag{3}$$

with ψ_n, ϵ_n, and $0 \le f_n \le 2$ being the KS orbitals, their energies and occupation numbers. Computationally, χ^0 and v in Eq. (2) can be interpreted as the matrix form of the non-interacting density response function and the bare Coulomb interaction, represented in terms of a set of suitable basis functions. For simplicity, here closed-shell systems (hence $f_n = 0$

or 2) and real orbitals are assumed. Extensions to spin-collinear cases and complex orbitals are straightforward.

Within an atomic-orbital (AO) basis set framework, the KS molecular orbitals (MOs) are expanded in terms of a set of atom-centered basis functions $\{\varphi_{i,\mathcal{I}}(\mathbf{r})\}$,

$$\psi_n(\mathbf{r}) = \sum_{i,\mathcal{I}} c^n_{i(\mathcal{I})} \varphi_{i,\mathcal{I}}(\mathbf{r} - \mathbf{R}_\mathcal{I}) \tag{4}$$

with $c^n_{i(\mathcal{I})}$ being the KS eigenvectors and $\mathbf{R}_\mathcal{I}$ the position of the atom $\mathcal{I}$, on which the basis function i is centering. For clarity, here we explicitly indicate the atom on which each atomic basis function belongs to, and the summation over i goes over only those AOs centering on the atom $\mathcal{I}$. Furthermore, the exact-exchange (EX) and RPA correlation energies are computed based on the RI approximation. Within this approximation, a set of auxiliary basis functions (ABFs) $\{P_\mu(\mathbf{r})\}$ are employed to expand the products of two AOs,

$$\varphi_{i,\mathcal{I}}(\mathbf{r} - \mathbf{R}_\mathcal{I})\varphi_{j,\mathcal{J}}(\mathbf{r} - \mathbf{R}_\mathcal{J}) = \sum_{\mu,\mathcal{U}} C^{\mu(\mathcal{U})}_{i(\mathcal{I}),j(\mathcal{J})} P_\mu(\mathbf{r} - \mathbf{R}_\mathcal{U}) \tag{5}$$

where $\mathbf{R}_\mathcal{U}$ is the position of the atom on which the ABF μ is centered, and $C^{\mu(\mathcal{U})}_{i(\mathcal{I}),j(\mathcal{J})}$ are the expansion coefficients, with the atoms to which the AOs and ABFs belong explicitly indicated in parenthesis.

In the global RI approximation,[53–56] the atom $\mathcal{U}$ could be a third atom other than the atoms $\mathcal{I}$ and $\mathcal{J}$; however, in the LRI approximation[46,57,58] adopted in the present work, $\mathcal{U}$ has to be either $\mathcal{I}$ or $\mathcal{J}$, i.e.,

$$\varphi_{i,\mathcal{I}}(\mathbf{r} - \mathbf{R}_\mathcal{I})\varphi_{j,\mathcal{J}}(\mathbf{r} - \mathbf{R}_\mathcal{J}) = \sum_{\mu\in\mathcal{I}} C^{\mu(\mathcal{I})}_{i(\mathcal{I}),j(\mathcal{J})} P_\mu(\mathbf{r} - \mathbf{R}_\mathcal{I}) + \sum_{\mu\in\mathcal{J}} C^{\mu(\mathcal{J})}_{i(\mathcal{I}),j(\mathcal{J})} P_\mu(\mathbf{r} - \mathbf{R}_\mathcal{J}) \tag{6}$$

where $\mu \in \mathcal{I}$ means the summation over ABFs $\{\mu\}$ are restricted to those centering on the atom $\mathcal{I}$. In the RI (LRI) formalism, another key quantity is the Coulomb matrix, which is

the representation of the Coulomb operator in terms of ABFs,

$$V_{\mu(\mathcal{U}),\nu(\mathcal{V})} = \int d\mathbf{r} d\mathbf{r}' \frac{P_\mu(\mathbf{r}-\mathbf{R}_\mathcal{U}) P_\nu(\mathbf{r}'-\mathbf{R}_\mathcal{V})}{|\mathbf{r}-\mathbf{r}'|} \,. \tag{7}$$

Introducing

$$O_{mn}^{\mu(\mathcal{U})} = \sum_{i,\mathcal{I}} \sum_{j,\mathcal{J}} \sum_{\nu,\mathcal{V}} c_{i(\mathcal{I})}^m C_{i(\mathcal{I}),j(\mathcal{J})}^{\nu(\mathcal{V})} c_{j(\mathcal{J})}^n \left[V^{\frac{1}{2}}\right]_{\nu(\mathcal{V}),\mu(\mathcal{U})} \tag{8}$$

where $V^{1/2}$ is the square root of the global Coulomb matrix, then it is straightforward to show that the exact-exchange energy is given by

$$E_x^{\mathrm{EX}} = -\sum_m^{occ} \sum_n^{occ} \sum_{\mu,\mathcal{U}} O_{mn}^{\mu(\mathcal{U})} O_{nm}^{\mu(\mathcal{U})} \,. \tag{9}$$

Further denoting

$$\mathbf{\Pi}_{\mu(\mathcal{U}),\nu(\mathcal{V})}(i\omega) = 2\sum_m^{occ} \sum_n^{unocc} \frac{2(\epsilon_m - \epsilon_n) O_{mn}^{\mu(\mathcal{U})} O_{nm}^{\nu(\mathcal{V})}}{(\epsilon_m-\epsilon_n)^2 + \omega^2} \tag{10}$$

(assuming integer occupations), the RPA correlation energy is then given by

$$E_c^{\mathrm{RPA}} = \frac{1}{2\pi} \int_0^\infty d\omega \mathrm{Tr}\left[\ln\left(\mathbf{1} - \mathbf{\Pi}(i\omega)\right) + \mathbf{\Pi}(i\omega)\right] \,. \tag{11}$$

More detailed derivations of Eqs. (9) and (11), on which our RPA force implementation is based, are given in Refs.[12,56]

From the above presentation, one can see that a key step in the RPA energy (and subsequently the RPA force) calculations is to evaluate the $O_{mn}^{\mu(\mathcal{U})}$ tensor, defined in Eq. (8). Previously, this was done rather straightforwardly in terms of matrix multiplications, without sufficiently exploiting the sparsity in $C_{i(\mathcal{I}),j(\mathcal{J})}^{\nu(\mathcal{V})}$. To facilitate a better parallelization efficiency and reduce the memory cost, we now change the strategy to calculate $O_{mn}^{\mu(\mathcal{U})}$ by taking into account the sparsity of $C_{i(\mathcal{I}),j(\mathcal{J})}^{\nu(\mathcal{V})}$. Specifically, using the property that $C_{i(\mathcal{I}),j(\mathcal{J})}^{\nu(\mathcal{V})}$ is nonzero only if $\mathcal{V} = \mathcal{I}$ or $\mathcal{V} = \mathcal{J}$ within the LRI, we first calculate an intermediate quantity,

given by local multiplication of $C^{\nu(\mathcal{V})}_{i(\mathcal{I}),j(\mathcal{J})}$ with the KS eigenvectors, i.e.,

$$\begin{aligned} S^{\nu(\mathcal{I})}_{i(\mathcal{I}),m} &= \sum_{j\in\mathcal{J}} C^{\nu(\mathcal{I})}_{i(\mathcal{I}),j(\mathcal{J})} c^{m}_{j(\mathcal{J})} \\ S^{\nu(\mathcal{I})}_{j(\mathcal{J}),m} &= \sum_{i\in\mathcal{I}} C^{\nu(\mathcal{I})}_{j(\mathcal{J}),i(\mathcal{I})} c^{m}_{i(\mathcal{I})} \end{aligned} \tag{12}$$

for each pair of atoms $\langle\mathcal{I},\mathcal{J}\rangle$ with $\mathcal{I}\geq\mathcal{J}$ and $\mathcal{V}=\mathcal{I}$. Similarly, we can calculate $S^{\nu(\mathcal{J})}_{i(\mathcal{I}),m}$ and $S^{\nu(\mathcal{J})}_{j(\mathcal{J}),m}$ for $\mathcal{V}=\mathcal{J}$.

With the intermediate quantity obtained, the target O-tensor can be calculated as

$$O^{\mu(\mathcal{U})}_{nm} = \sum_{\mathcal{J}\mathcal{V}} \sum_{j\in\mathcal{J},\nu\in\mathcal{V}} c^{n}_{j(\mathcal{J})} S^{\nu(\mathcal{V})}_{j(\mathcal{J}),m} \left[V^{\frac{1}{2}}\right]_{\nu(\mathcal{V}),\mu(\mathcal{U})} \tag{13}$$

This step helps a lot to deal with the storage of the three-index C tensor and its transformation to MO representations.

2.2 RPA Forces within the LRI Framework

The force that an atom feels due to the RPA correlation energy is the negative of the gradient of RPA correlation energy, i.e.,

$$\begin{aligned} F^{\mathrm{RPA}}_{c,A} = -\frac{dE^{\mathrm{RPA}}_c}{d\mathbf{R}_A} &= -\Big\langle \frac{dE^{\mathrm{RPA}}_c}{dC}\frac{dC}{d\mathbf{R}_A}\Big\rangle - \Big\langle \frac{dE^{\mathrm{RPA}}_c}{dV}\frac{dV}{d\mathbf{R}_A}\Big\rangle - \Big\langle \frac{dE^{\mathrm{RPA}}_c}{dc}\frac{dc}{d\mathbf{R}_A}\Big\rangle - \Big\langle \frac{dE^{\mathrm{RPA}}_c}{d\epsilon}\frac{d\epsilon}{d\mathbf{R}_A}\Big\rangle \\ &= \Big\langle \Gamma^{(1)}\frac{dC}{d\mathbf{R}_A}\Big\rangle + \Big\langle \Gamma^{(2)}\frac{dV}{d\mathbf{R}_A}\Big\rangle + \Big\langle \Gamma^{(3)}\frac{dc}{d\mathbf{R}_A}\Big\rangle + \Big\langle \Gamma^{(4)}\frac{d\epsilon}{d\mathbf{R}_A}\Big\rangle, \end{aligned} \tag{14}$$

where the first two terms depend on the atomic positions explicitly, while the last two terms, consisting of the analytical gradients of KS eigenvectors and eigenenergies, depend on the atomic positions implicitly and are obtained via density-functional perturbation theory (DFPT).[59] In practical calculations, we introduce two frequency-integrated intermediate

quantities,

$$\Upsilon^{\mu(\mathcal{U})}_{mn} = \int_0^\infty \frac{d\omega}{2\pi} \times \Big(\sum_{\nu,\mathcal{V}} \frac{f_m - f_n}{\epsilon_m - \epsilon_n - i\omega} O^{\nu(\mathcal{V})}_{mn} \mathbf{W}^c_{\nu(\mathcal{V}),\mu(\mathcal{U})}(i\omega) \Big) \tag{15}$$

and

$$\tilde{\Upsilon}^{\mu(\mathcal{U})}_{mn} = \int_0^\infty \frac{d\omega}{2\pi} (f_m - f_n) \times \Big(\sum_{\nu,\mathcal{V}} \frac{2\left[\omega^2 - (\epsilon_m - \epsilon_n)^2\right]}{\left[(\epsilon_m - \epsilon_n)^2 + \omega^2\right]^2} O^{\nu(\mathcal{V})}_{mn} \mathbf{W}^c_{\nu(\mathcal{V}),\mu(\mathcal{U})}(i\omega) \Big) \tag{16}$$

where

$$\mathbf{W}^c(i\omega) = \left[\frac{\mathbf{\Pi}(i\omega)}{\mathbf{1} - \mathbf{\Pi}(i\omega)} \right], \tag{17}$$

with $\mathbf{\Pi}$ defined in Eq. (10). Then, for the case of integer occupations, the $\Gamma^{(n)}$ tensors introduced in Eq. (14) can be evaluated as

$$\begin{aligned} \Gamma^{(1)}_{i(\mathcal{I})j(\mathcal{J}),\mu(\mathcal{U})} &= -\frac{dE_c^{\mathrm{RPA}}}{dC^{\mu(\mathcal{U})}_{i(\mathcal{I}),j(\mathcal{J})}} = \sum_{\nu,\mathcal{V}} V^{\frac{1}{2}}_{\mu(\mathcal{U}),\nu(\mathcal{V})} \sum_{m,n} c^m_{i,\mathcal{I}} \Upsilon^{\nu(\mathcal{V})}_{mn} c^n_{j,\mathcal{J}} \\ &= \sum_{\nu,\mathcal{V}} V^{\frac{1}{2}}_{\mu(\mathcal{U}),\nu(\mathcal{V})} \sum_{m}^{occ} \sum_{n}^{unocc} \left[c^m_{i,\mathcal{I}} \Upsilon^{\nu(\mathcal{V})}_{mn} c^n_{j,\mathcal{J}} + c^n_{i,\mathcal{I}} \Upsilon^{\nu(\mathcal{V})}_{nm} c^m_{j,\mathcal{J}} \right] \end{aligned} \tag{18}$$

$$\Gamma^{(2)}_{\mu(\mathcal{U}),\nu(\mathcal{V})} = -\frac{dE_c^{\mathrm{RPA}}}{dV_{\mu(\mathcal{U}),\nu(\mathcal{V})}} = \sum_{\mu',\mathcal{U}'} \sum_{\nu',\mathcal{V}'} V^{-\frac{1}{2}}_{\mu(\mathcal{U}),\mu'(\mathcal{U}')} \Big(\sum_{m}^{occ} \sum_{n}^{unocc} O^{\mu'(\mathcal{U}')}_{mn} \Upsilon^{\nu'(\mathcal{V}')}_{nm} \Big) V^{-\frac{1}{2}}_{\nu'(\mathcal{V}'),\nu(\mathcal{V})} , \tag{19}$$

$$\Gamma^{(3)}_{i(\mathcal{I}),m} = -\frac{dE_c^{\mathrm{RPA}}}{dc^m_{i(\mathcal{I})}} = 2 \sum_n \sum_{j,\mathcal{J}} \sum_{\nu,\mathcal{V}} Q^{\nu(\mathcal{V})}_{i(\mathcal{I}),j(\mathcal{J})} c^n_{j(\mathcal{J})} \Upsilon^{\nu(\mathcal{V})}_{nm} , \tag{20}$$

with

$$Q^{\nu(\mathcal{V})}_{i(\mathcal{I}),j(\mathcal{J})} = \sum_{\mu,\mathcal{U}} C^{\mu(\mathcal{U})}_{i(\mathcal{I}),j(\mathcal{J})} \left[V^{\frac{1}{2}} \right]_{\mu(\mathcal{U}),\nu(\mathcal{V})} \tag{21}$$

and

$$\Gamma_m^{(4)} = -\frac{dE_c^{\mathrm{RPA}}}{d\epsilon_m} = \sum_n \sum_{\nu,\mathcal{V}} O_{mn}^{\nu(\mathcal{V})} \tilde{\Upsilon}_{mn}^{\nu(\mathcal{V})} \,. \tag{22}$$

Further details of the derivation of these equations can be found in Ref. 35, although we have used slightly different notations here by explicitly specifying the atomic positions of the AOs and ABFs. For N_{at} total atoms, there should be $N_{at}(N_{at}-1)/2$ atom pairs which constitute the upper/lower triangular part of a matrix. For onsite atom pairs, the derivatives are zero and so does the force.

Next, we briefly explain how the traces in Eq. (14) is performed. First, we note that the global trace operation can be separated into a summation over atomic pairs,

$$\big\langle AB \big\rangle = 2 \sum_{\mathcal{I}>\mathcal{J}} \big\langle AB \big\rangle_{\langle \mathcal{I},\mathcal{J} \rangle} \tag{23}$$

and for each pair, we perform local multiplications over the orbital indices. In fact, this separation is most convenient for the first two terms in Eq. 14, involving the derivatives of expansion coefficients C and the Coulomb matrix V with respect to the atomic positions. Taking the first term for example, for each atomic pair $\langle \mathcal{I}, \mathcal{J} \rangle$, the following local operations are performed, utilizing the sparse property of $C_{i(\mathcal{I}),j(\mathcal{J})}^{\mu(\mathcal{U})}$,

$$\big\langle \Gamma^{(1)} \frac{dC}{d\mathbf{R}_A} \big\rangle_{\langle \mathcal{I},\mathcal{J} \rangle} = \sum_{\mu \in \mathcal{I}} \sum_{i \in \mathcal{I}, j \in \mathcal{J}} \Gamma^{(1)}_{i(\mathcal{I})j(\mathcal{J}),\mu(\mathcal{I})} \frac{dC^{\mu(\mathcal{I})}_{j(\mathcal{J}),i(\mathcal{I})}}{d\mathbf{R}_A} + \sum_{\mu \in \mathcal{J}} \sum_{i \in \mathcal{I}, j \in \mathcal{J}} \Gamma^{(1)}_{i(\mathcal{I})j(\mathcal{J}),\mu(\mathcal{J})} \frac{dC^{\mu(\mathcal{J})}_{j(\mathcal{J}),i(\mathcal{I})}}{d\mathbf{R}_A} \,, \tag{24}$$

which amounts to two separate contractions over small rank-3 tensors.

Similarly, for the second term, we have

$$\left\langle \Gamma^{(2)} \frac{dV}{d\mathbf{R}_A} \right\rangle_{\langle \mathcal{I},\mathcal{J} \rangle} = \sum_{\mu \in I} \sum_{\nu \in J} \Gamma^{(2)}_{\mu(\mathcal{I}),\nu(\mathcal{J})} \frac{dV_{\nu(\mathcal{J}),\mu(\mathcal{I})}}{d\mathbf{R}_A} \tag{25}$$

Briefly, by exploiting the sparsity and symmetry properties of the intermediate quantities, the RPA force calculations can be substantially sped up, and the storage requirement is considerably reduced. The key operations discussed above are summarized in the algorithm presented in Algorithm. 1.

Algorithm 1 Flowchart for efficient evaluation of the O^{μ}_{nm} tensor and $\langle \Gamma^{(1)} \frac{dC}{dR} \rangle$. Here N_{at}, N_b, N_{occ}, N_{unocc}, N_{aux}, $\mu(\mathcal{I})$, and $i(\mathcal{I})$ are the numbers of atoms, the AO basis functions, the occupied states, the unoccupied states, the total ABFs, and an ABF and AO belonging to the atom $\mathcal{I}$, respectively. In practical calculations, $N_{aux} > N_b = N_{occ} + N_{unocc} > N_{unocc} > N_{occ}$. For calculation of O^{μ}_{ij}, only $N\_pairs = N_{at}(N_{at}+1)/2$ atomic pairs are needed, under the restriction of $\mathcal{I} \geq \mathcal{J}$.

$O^{\mu(\mathcal{U})}_{nm} = 0$; $\quad F^{\mathrm{RPA}}_{c,A} = 0$

for $\mathcal{K} \leftarrow 1$ to N_pairs **do**

  $\mathcal{I}$: first atom in pair, $\mathcal{J}$: second atom in pair, $\mathcal{I} \geq \mathcal{J}$

  Compute $C^{\nu(\mathcal{I})}_{i(\mathcal{I}),j(\mathcal{J})}$ & $C^{\nu(\mathcal{J})}_{i(\mathcal{I}),j(\mathcal{J})}$

  $S^{\nu(\mathcal{I})}_{i(\mathcal{I}),m} \leftarrow \sum_{j,\mathcal{J}} C^{\nu(\mathcal{I})}_{i(\mathcal{I}),j(\mathcal{J})} c^{m}_{j(\mathcal{J})}$ (cf. Eq. 12)

  $S^{\nu(\mathcal{I})}_{j(\mathcal{J}),m} \leftarrow \sum_{i,\mathcal{I}} C^{\nu(\mathcal{I})}_{i(\mathcal{I}),j(\mathcal{J})} c^{m}_{i(\mathcal{I})}$ (cf. Eq. 12)

  $S^{\nu(\mathcal{J})}_{i(\mathcal{I}),m} \leftarrow \sum_{j,\mathcal{J}} C^{\nu(\mathcal{J})}_{i(\mathcal{I}),j(\mathcal{J})} c^{m}_{j(\mathcal{J})}$

  $S^{\nu(\mathcal{J})}_{j(\mathcal{J}),m} \leftarrow \sum_{i,\mathcal{I}} C^{\nu(\mathcal{J})}_{i(\mathcal{I}),j(\mathcal{J})} c^{m}_{i(\mathcal{I})}$

end for

$O^{\mu(\mathcal{U})}_{nm} \leftarrow \sum_{j,\mathcal{J}} \sum_{\nu,\mathcal{V}} c^{n}_{j(\mathcal{J})} \; S^{\nu(\mathcal{V})}_{j(\mathcal{J}),m} \left[V^{\frac{1}{2}} \right]_{\nu(\mathcal{V})\mu(\mathcal{U})}$ (cf. Eq. 13)

$\overline{\Gamma}^{(1)}_{i(\mathcal{I}),m,\mu(\mathcal{U})} = \sum_{\nu,\mathcal{V}} \sum_{n}^{unocc} V^{\frac{1}{2}}_{\mu(\mathcal{U}),\nu(\mathcal{V})} \Upsilon^{\nu(\mathcal{V})}_{mn} c^{n}_{i(\mathcal{I})}$ (cf. Eq. 18)

for $\mathcal{K} \leftarrow 1$ to N_pairs **do**

  $\mathcal{I}$: first atom in pair, $\mathcal{J}$: second atom in pair, $\mathcal{I} > \mathcal{J}$

  Compute $\dfrac{dC^{\mu(\mathcal{I})}_{i(\mathcal{I}),j(\mathcal{J})}}{dR_{\mathcal{I}\mathcal{J}}}$ & $\dfrac{dC^{\mu(\mathcal{J})}_{i(\mathcal{I}),j(\mathcal{J})}}{dR_{\mathcal{I}\mathcal{J}}}$

  $\Gamma^{(1)}_{i(\mathcal{I}),j(\mathcal{J}),\mu(\mathcal{I})} \leftarrow \sum_{m}^{occ} c^{m}_{i(\mathcal{I})} \overline{\Gamma}^{(1)}_{j(\mathcal{J}),m,\mu(\mathcal{I})}$ (cf. Eq. 18)

  $\Gamma^{(1)}_{i(\mathcal{I}),j(\mathcal{J}),\mu(\mathcal{I})} \leftarrow \Gamma^{(1)}_{i(\mathcal{I}),j(\mathcal{J}),\mu(\mathcal{I})} + \sum_{m}^{occ} \overline{\Gamma}^{(1)}_{i(\mathcal{I}),m,\mu(\mathcal{I})} c^{m}_{j(\mathcal{J})}$ (cf. Eq. 18)

  $F^{\mathrm{RPA}}_{c,\mathcal{I}} \leftarrow F^{\mathrm{RPA}}_{c,\mathcal{I}} - 2 \sum_{i,\mathcal{I},\ j,\mathcal{J},\ \mu,\mathcal{I}} \dfrac{dC^{\mu(\mathcal{I})}_{i(\mathcal{I}),j(\mathcal{J})}}{dR_{\mathcal{I}\mathcal{J}}} \Gamma^{(1)}_{i(\mathcal{I}),j(\mathcal{J}),\mu(\mathcal{I})}$

  $F^{\mathrm{RPA}}_{c,\mathcal{J}} \leftarrow F^{\mathrm{RPA}}_{c,\mathcal{J}} + 2 \sum_{i,\mathcal{I},\ j,\mathcal{J},\ \mu,\mathcal{I}} \dfrac{dC^{\mu(\mathcal{I})}_{i(\mathcal{I}),j(\mathcal{J})}}{dR_{\mathcal{I}\mathcal{J}}} \Gamma^{(1)}_{i(\mathcal{I}),j(\mathcal{J}),\mu(\mathcal{I})}$

  $\Gamma^{(1)}_{i(\mathcal{I}),j(\mathcal{J}),\mu(\mathcal{J})} \leftarrow \sum_{m}^{occ} c^{m}_{i(\mathcal{I})} \overline{\Gamma}^{(1)}_{j(\mathcal{J}),m,\mu(\mathcal{J})}$ (cf. Eq. 18)

  $\Gamma^{(1)}_{i(\mathcal{I}),j(\mathcal{J}),\mu(\mathcal{J})} \leftarrow \Gamma^{(1)}_{i(\mathcal{I}),j(\mathcal{J}),\mu(\mathcal{J})} + \sum_{m}^{occ} \overline{\Gamma}^{(1)}_{i(\mathcal{I}),m,\mu(\mathcal{J})} c^{m}_{j(\mathcal{J})}$ (cf. Eq. 18)

  $F^{\mathrm{RPA}}_{c,\mathcal{I}} \leftarrow F^{\mathrm{RPA}}_{c,\mathcal{I}} - 2 \sum_{i,\mathcal{I},\ j,\mathcal{J},\ \mu,\mathcal{J}} \dfrac{dC^{\mu(\mathcal{J})}_{i(\mathcal{I}),j(\mathcal{J})}}{dR_{\mathcal{I}\mathcal{J}}} \Gamma^{(1)}_{i(\mathcal{I}),j(\mathcal{J}),\mu(\mathcal{J})}$

  $F^{\mathrm{RPA}}_{c,\mathcal{J}} \leftarrow F^{\mathrm{RPA}}_{c,\mathcal{J}} + 2 \sum_{i,\mathcal{I},\ j,\mathcal{J},\ \mu,\mathcal{J}} \dfrac{dC^{\mu(\mathcal{J})}_{i(\mathcal{I}),j(\mathcal{J})}}{dR_{\mathcal{I}\mathcal{J}}} \Gamma^{(1)}_{i(\mathcal{I}),j(\mathcal{J}),\mu(\mathcal{J})}$

end for

2.3 Computational details

The improved algorithm for RPA gradient calculations as discussed above has been implemented in the FHI-aims code package.[56,60,61] In our calculations, we consider water clusters of size n =21, 22, 25 for determining the energy ordering of low-lying isomers. A modified Gauss-Legendre frequency grid with sufficient mesh points is used for frequency integration in RPA force and single-point energy calculations. Frozen-core approximation is used for RPA, RPA+rSE and MP2 calculations unless otherwise stated. The convergence criterion for geometry relaxation is set to 10^{-2} eV/Å. In FHI-aims both NAO and GTO basis sets can be used. In the present work, to facilitate the comparison with quantum chemistry literature, the GTO basis sets cc-pVTZ short (TZ), aug-cc-pVTZ (aTZ), cc-pVQZ (QZ) are used in the calculations. Furthermore, for RPA single-point energy calculations, an additional $5g$ hydrogen-like functions (with effective charge Z = 6) is used to generate extra ABFs (the "for_aux" tag in FHI-aims)[46,62] to improve the accuracy of local RI. The gas-phase equilibrium geometry of H_2O monomer with TTM2-F has (R_{O-H}) 0.9578 Å, and (θ) 104.51°.[63]

3 Results and Discussions

The inter-molecular interaction between water molecules is of great interest in many fields of science. As mentioned above, the RPA is an appealing approach for describing the energetic and structural properties of water clusters. Developing efficient algorithms for RPA gradient calculations is hence a key step towards turning the RPA into a powerful tool for simulating properties of water systems. In this section, we present the major results of the present work, including a benchmark comparison with literature results, the scaling behavior of our RPA gradient implementation with respect to system size, and the energy ordering and structural parameters of a sequence of water clusters.

3.1 Benchmark results for the $(H_2O)_{20}$ clusters

To start with, we examine the numerical precision of our RPA calculations for medium-sized water clusters by comparing our RPA results for the low-lying isomers of $(H_2O)_{20}$ clusters with those of Chedid *et al.*,[34] obtained using Gaussian cc-pVTZ and cc-pVQZ basis sets. In Table 1, we present the RPA@PBE total energies for four isomers of $(H_2O)_{20}$ clusters calculated in the present work, in comparison with those reported in Ref. 34. In our calculations, two sets of geometries are used, i.e., the geometries provided along with the WATER27 testset, obtained at the hybrid functional B3LYP level, and the geometries fully relaxed at the level of RPA@PBE. The former set of results are in excellent agreement with those reported in Ref. 34. The total energies can differ up to 1-2 mH, but the energy differences between the different isomers are significantly below 0.1 mH, indicating that the original WATER27 geometries were also used in the calculations of Ref. 34. Naturally, the energy orderings among the four isomers predicted by the two implementations are consistent with each other, ending up with a sequence of "Edge-sharing" < "Face-sharing" < "Face-cubes" < "Dodecahedron",[34,48] if the cc-pVQZ basis set is used. However, as shown in Table 1, the energy ordering of the "Face-sharing" and "Face-cubes" isomers will be swapped when using the smaller cc-pVTZ basis set. Again, both implementations consistently predicted such a basis set dependence of the RPA energy ordering, which signifies that high-quality basis sets are needed to obtain even qualitatively reliable RPA results. For comparison, in Table 1 we also present the RPA@PBE results obtained using the RPA geometries. Now the energy differences (shown in parenthesis) obtained using the WATER27 and RPA geometries differ by 0.3 - 2 mH, but the energy ordering does not change. Finally, as a side remark, one may notice that the RPA energies obtained using RPA geometries are slightly higher than RPA energies with WATER27 geometries, in contrast with one would expect. This is because the RPA geometries are relaxed in the all-electron manner, while the RPA energies are obtained using the frozen-core approximation.

Table 1: Comparison of the RPA@PBE energies (in Hartree) for the four $(H_2O)_{20}$ isomers with the literature values reported by Chedid *et al.*,[34] using both cc-pVTZ and cc-pVQZ basis sets. The energy differences from the lowest-energy (Edge-sharing) isomer are given in parenthesis. In the present work, both the original WATER27 geometries (indicated by the superscript b) and the fully-relaxed all-electron RPA geometries (indicated by c) are used.

basis set	Edge-sharing	Face-sharing	Face-cubes	Dodecahedron
cc-pVTZ[a]	**−1529.399108**	−1529.397262 (0.001846)	−1529.397983 (0.001125)	−1529.378167 (0.020941)
cc-pVQZ[a]	**−1530.258903**	−1530.256714 (0.002189)	−1530.256446 (0.002457)	−1530.241595 (0.017308)
cc-pVTZ[b]	**−1529.401778**	−1529.399957 (0.001821)	−1529.400688 (0.001090)	−1529.380768 (0.021010)
cc-pVQZ[b]	**−1530.260364**	−1530.258183 (0.002181)	−1530.257954 (0.002410)	−1530.243048 (0.017316)
cc-pVTZ[c]	**−1529.401790**	−1529.399549 (0.002241)	−1529.399979 (0.001811)	−1529.381531 (0.020259)
cc-pVQZ[c]	**−1530.258408**	−1530.255937 (0.002471)	−1530.255528 (0.002880)	−1530.243154 (0.015254)

[a]Ref 34 [b]This work (WATER27 geometries)) [c]This work (RPA geometries)

3.2 Scaling behavior of the computational cost

The computational efficiency of our RPA gradient implementation has been significantly improved since its first publication in Ref. 35. To check the scaling behavior of our improved implementation, we have considered water clusters $(H_2O)_n$ of increasing size ranging from $n = 20$ to 139. In Fig. 1, we plot the computational timings for one iteration of RPA geometry relaxation as a function of n. A polynomial fit of the data points shows that the scaling behavior of the computational time is well described by $t(n) = bn^{\alpha}$ with $\alpha = 2.6$. Such a sub-cubic scaling is a significant improvement over the original $O(N^4)$-scaling algorithm, achieved by further exploiting the sparsity of the integrals offered by the atomic-orbital basis sets and LRI scheme, as described in Sec. 2.1 and 2.2.

3.3 Basis set convergence

The basis set convergence of the RPA for water clusters has been thoroughly examined in Ref. 34 based on the benchmark results on the WATER27[64] testset, which contains neutral, protonated, and deprotonated water clusters up to $n = 20$. There, it is found that the RPA underbinds the water clusters substantially at finite basis sets, and this underbinding behavior becomes even more severe as one approaches the complete basis set (CBS) limit.

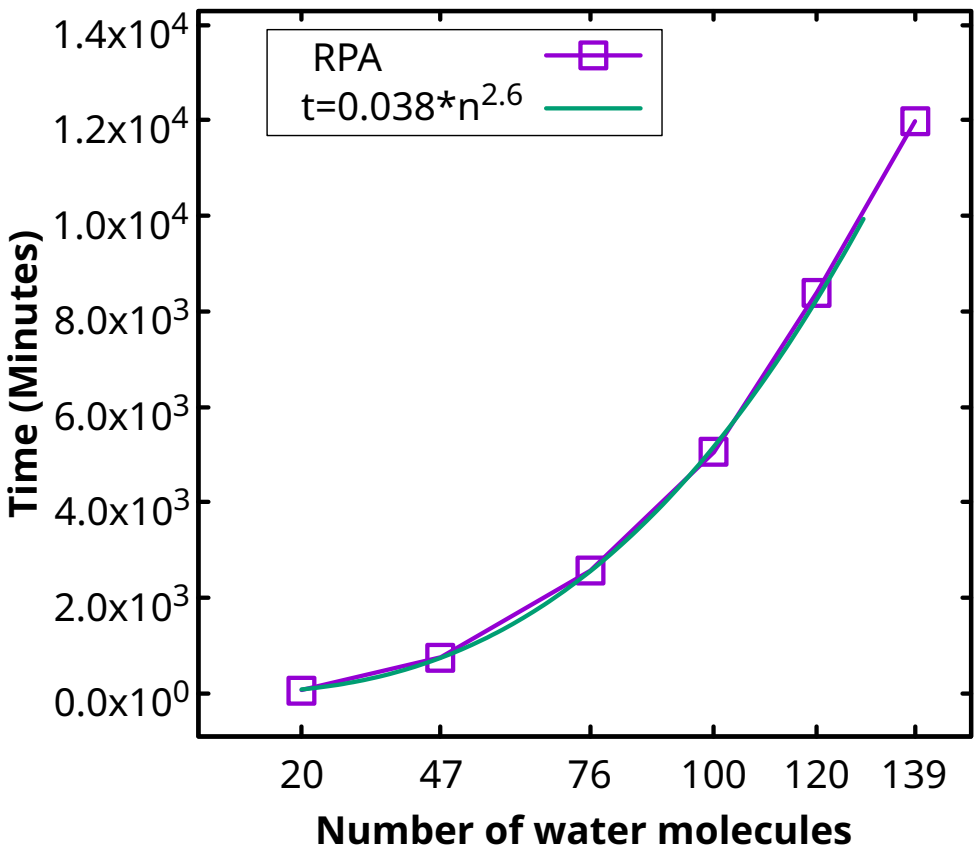

Figure 1: Wall-clock timings (in minutes) of one RPA relaxation step as a function of the water cluster size n. The Gaussian cc-pVTZ basis sets are used. The calculations were performed on 320 CPU cores. A polynomial fit of the scaling behavior of the computational times is also added to the graph.

The RPA binding strength for water clusters, if not corrected for the basis set superposition errors (BSSEs), becomes gradually weaker as the basis size increases. On the contrary, if the BSSEs are corrected, the RPA binding energies converge from the opposite direction. Such behaviors for the binding energies are illustrated in Fig. 2 for the water dimer case. The final extrapolated CBS(5,6) results with and without counterpoise corrections are fairly close, differing only by approximately 0.1 kcal/mol for the water dimer (cf. Fig. 2).

Our interest here is to investigate what happens for the RPA+rSE method which has been shown to largely remedy the underbinding problem of the RPA for weakly bonded molecules.[25] In Table 2, we present the deviations of both the RPA and RPA+rSE (BSSE-uncorrected) binding energies, obtained using both def2-QZVPP and cc-pV5Z/cc-pV6Z basis

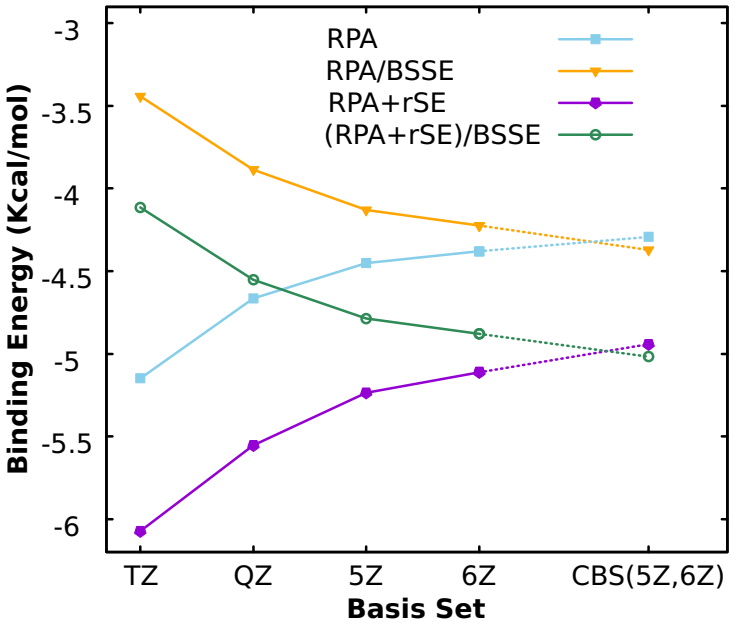

Figure 2: Convergence of the RPA@PBE and (RPA+rSE)@PBE binding energies for the water dimer with respect to the basis size. The Dunning's cc-pVnZ basis sets are used in the tests. Binding energies with and without counterpoise corrections are both shown.

sets, from the reference values for WATER27 testset. The reference values are obtained using the coupled cluster theory with single, double, and perturbative triple excitations (CCSD(T)), with dedicated efforts to achieve convergence with respect to basis size. We note that, in this work, the binding energies of water clusters are defined as

$$E_{\rm b} = -\left[E((\mathrm{H_2O})_n) - nE(\mathrm{H_2O})\right] \tag{26}$$

and hence a larger positive number means stronger binding and lower total energy of an isomer. As shown in Table 2, our RPA results are in excellent agreement with those reported in Ref.[34] The RPA+rSE results, first calculated in the present work, show interesting features. At finite basis sets, the RPA+rSE, without correcting BSSEs, exhibits opposite behavior as RPA, i.e., it overbinds the water clusters. However, the amount of overbinding gets smaller as the basis size increases, and the extrapolated CBS(5Z,6Z) results on average only deviate by about 1.4 kcal/mol from the reference values. Such an accuracy is on a paar

with the performance of the state-of-the-art double hybrid functional DSD-BLYP[65] with additional dispersion corrections. Unfortunately, it should be noted that the performance of RPA+rSE, similar to RPA, has a strong basis set dependence, and such an accuracy can only be achieved at the CBS limit.

Table 2: Mean deviations (MDs), mean absolute deviations (MADs), and maximum absolute deviations (Max) in kcal/mol of the reference energies provides by Manna *et al.*[66] for the WATER27 benchmark set structures[64] with (optimized geometries B3LYP/6-311++G(2d,2p) for various methods using def2-QZVPP(QZVPP) basis set. The negative error means the binding energies are underestimated.

Method	MD	MAD	MAX
RPA@PBE [QZVPP][a]	−2.90	4.90	16.400
RPA@PBE [QZVPP][b]	−2.74	5.02	16.339
(RPA+rSE)@PBE [QZVPP][b]	7.89	7.89	18.190
RPA@PBE [5Z][b]	-3.78	5.31	18.766
RPA@PBE [6Z][b]	-5.52	5.74	21.540
(RPA+rSE)@PBE [5Z][b]	6.76	6.76	15.351
(RPA+rSE)@PBE [6Z][b]	4.40	4.40	10.864
RPA@PBE [CBS(5Z,6Z)][a]	-7.40	7.40	25.900
RPA@PBE [CBS(5Z,6Z)][b]	-7.64	7.64	25.820
(RPA+rSE)@PBE [CBS(5Z,6Z)][b]	1.40	1.41	4.221
M06-2X-D3(0)	3.40	3.70	10.000
ωB97X-D3(0)	2.20	2.30	7.400
DSD-BLYP-D3(0)	1.20	1.30	5.500

[a]Ref 34 [b]This work (results obtained using FHI-aims)

3.4 Energy hierarchy for low-lying isomers of $(H_2O)_n$ clusters with n=21, 22, 25

The energy landscapes of putative and low-lying minima of water clusters of n = 3-25 have been thoroughly studied in Ref. 67 using the TTM2.1-F force field (Thole Type Model version 2.1 for Flexible monomers).[68] Our concern here is if and how the energy ordering of the low-lying isomers determined by the force field will change when the RPA method is applied. As an illustration, here we only consider a collection of 9 isomers of water clusters of size n =21, 22, and 25, taken from the Database of Water Cluster Minima.[67] These

include two low-lying isomers of $n = 21$ and 22, and five low-lying ones of $n = 25$. For these isomers, we have fully relaxed the structures using PBE, PBE0, and RPA with cc-pVQZ basis set. The (RPA+rSE)@PBE energy calculations are performed using the relaxed RPA@PBE structures. The energy calculations for these methods are performed using the same cc-pVQZ basis set. The obtained PBE, PBE0, RPA@PBE, and (RPA+rSE)@PBE results are presented in Table 3 and 4, together with those of TTM2.1-F and MP2 methods reported in the literature.[67] Here, the MP2 results, taken from Ref.,[67] are obtained using the aug-cc-pVTZ basis set.

Table 3 presents the computed binding energies for water clusters $n = 21$ and 22, with two isomers (denoted as a and b) for each size. These two isomers are chosen since they are energetically the lowest ones within 1 KJ/mol as determined by the TTM2.1-F force field. In Table 3, the lower-energy isomer of the two clusters is highlighted in bold for each method and the energy difference between the two isomers is given in parenthesis. For the cluster size $n = 21$, one can see that TTM2.1-F, PBE, and PBE0 predict that a is lowest-energy isomer, whereas MP2, RPA, and RPA+rSE instead favors the isomer b. This highlights the importance of including non-local electron correlations in the calculations for water clusters. To check the influence of the underlying geometries on the energy ordering, we carried out a crosscheck by performing RPA energy calculations on top of the TTM2.1-F force-field geometry, and by performing MP2 calculations on top of the TTM2.1-F and RPA geometries. Interestingly, as indicated in Table 3, if RPA or MP2 calculations were not performed on their own geometries, the isomer a is again favored. This signifies the high sensitivity of the water cluster structures to the employed computational methods, which in turn influences the energy hierarchy for the energetically very close isomers (within 1 KJ/mol).

For $n = 22$, all methods consistently predict that the isomer a is the putative minimum, although the actual energy differences scatter a lot, depending on the computational methods and/or the employed geometries. Quantitatively, however, it seems that the energy differ-

ences based on RPA@PBE geometries ($\sim$ 1.1 - 1.5 kcal/mol) are noticeably larger than other cases (0.07 - 0.23 kcal/mol). Considering the magnitude of binding energies themselves, the results yielded by different methods vary a lot. This is partly because the binding energies obtained using cc-pVQZ basis set are not yet converged. In particular, it can be noticed that RPA generally tends to underbind the water clusters, yielding a relatively smaller binding energies compared to other methods, e.g., MP2. Upon including the rSE correction, the magnitude of the binding energies is increased as much as 40 kcal/mol for this size of water clusters. This is similar to the case of water hexamers, where adding the rSE correction to RPA increases the binding energy by more than 1 kcal/mol per H_2O molecule.[35]

Table 3: Binding energies E_b (in kcal/mol) obtained by TTM2.1-F (force field), PBE, PBE0, MP2, RPA and RPA+rSE. The results of the lower-energy isomer are highlighted in bold for each method, and the binding energy differences between the two isomers are given in parenthesis. The geometries used in the energy calculations are explicitly indicated. The cc-pVQZ (QZ) basis set is used for all these calculations, except for PBE and MP2 calculations where the aug-cc-pVTZ (aTZ) basis set is also used.

method	$n = 21$		$n = 22$	
	a	b	a	b
Own Geometries				
TTM2.1-F[a]	**227.785**	227.565 (0.220)	**239.167**	239.099 (0.068)
MP2/aTZ[a]	232.618 (0.126)	**232.744**	**242.833**	242.701 (0.132)
PBE/aTZ	**228.217**	228.139 (0.078)	**235.183**	234.976 (0.207)
PBE	**259.651**	259.564 (0.087)	**268.978**	268.749 (0.229)
PBE/light	**251.457**	251.415 (0.042)	**259.657**	259.262 (0.395)
PBE/tight	**227.940**	227.867 (0.073)	**234.940**	234.694 (0.246)
PBE0	**239.762**	239.652 (0.110)	**248.541**	248.423 (0.118)
Geometry optimization RPA@PBE				
RPA@PBE	210.818 (0.058)	**210.876**	**219.609**	218.209 (1.400)
MP2	**241.947**	241.795 (0.152)	**252.101**	250.991 (1.110)
(RPA+rSE)@PBE	250.938 (0.049)	**250.987**	**263.539**	262.208 (1.459)
Geometry optimization TTM2.1-F[a]				
RPA@PBE	**207.612**	207.323 (0.289)	**216.724**	216.578 (0.146)
MP2	**236.485**	236.183 (0.302)	**246.829**	246.768 (0.061)

[a]Ref[67]

In Table 4, we further present the binding energy results for water clusters of $n = 25$, obtained using various methods. In this case, there are five low-lying isomers, for which the energy ordering is also of great interest, in analogy to the water hexamer case.[9,35] Again, in Table 4, the lowest-energy isomer is highlighted in bold, and the energy differences between other isomers and the lowest-energy one are given in parenthesis. For RPA@PBE energies, the binding energies are calculated under three sets of geometries: the TTM2.1-F force-field geometry, the PBE geometry, and RPA@PBE geometry. Although the isomer b is always the lowest-energy one for all three sets of geometries, the actual energy orderings are different. For example, using its own geometries, the RPA@PBE predicts an energy ordering of $b < e < a < c < d$, whereas a different energy ordering of $b < a < e < c < d$ is obtained if the PBE geometry is used. The energy ordering is again different under the TTM2.1-F geometry. The situation here is different from what happens for the water hexamer, where using PBE or RPA@PBE geometries won't lead to a qualitatively different energy ordering.[35] A similar effect is also observed for MP2, where using RPA@PBE or TTM2.1-F geometries for MP2 calculations also leads to a different energy ordering, as can be seen from Table 4. Compared to the water hexamer and dodecamer, here we are dealing with five isomers with the same structural motif (the O skeleton) and having even smaller energy differences (per water molecule). Hence the structural sensitivity of the energy ordering is much more pronounced here.

In Fig. 3, we plot the variation in the binding energies of the five isomers where the isomer b is taken as the reference (whose binding energy is set to zero for all methods). Here, the calculations of all methods are performed under their own geometries, except for MP2 and RPA+rSE for which the calculations are done under the RPA@PBE geometries. The isomers on the x-axis are ordered decreasingly ($b \to e \to a \to c \to d$) according to the RPA binding energies evaluated on the RPA geometries. Figure 3 indicates that these isomers are very close in energy at the level of the TTM2.1-F force-field method, but show much larger variations when one goes to first-principles methods. Furthermore, PBE and PBE0 show

similar variation patterns across the five isomers, which are however quite different from the behaviors of MP2 and RPA-based methods. Among MP2, RPA, and RPA+rSE, the former two essentially yield the same results, whereas RPA+rSE shows noticeable differences. In particular, compared to RPA and MP2, the order of isomers a and e is swapped in RPA+rSE. It is still not clear if this ordering change upon including rSE correction agrees with more accurate quantum chemistry approach such as CCST(T) or not. More investigations along this line are needed.

Table 4: Binding energies E_b (in kcal/mol) of the five low-lying isomers of $(H_2O)_25$ clusters obtained by TTM2.1-F (force field), PBE, PBE0, MP2, RPA and RPA+rSE. The binding energies of the lowest-energy isomer are highlighted in bold for each method, and the differences between other isomers and lowest-energy one are given in parenthesis. The geometries used in the energy calculations are explicitly indicated. The cc-pVQZ basis set is used for all these calculations.

method	$n = 25$				
	a	b	c	d	e
TTM2.1-F[a]	**277.472**	277.451 (0.021)	277.421 (0.051)	277.346 (0.126)	277.329 (0.143)
PBE0	290.637 (0.790)	**291.427**	289.814 (1.613)	289.711 (1.716)	289.981 (1.446)
Geometry optimization PBE					
PBE	314.258 (0.907)	**315.165**	313.310 (1.855)	313.256 (1.909)	313.522 (1.643)
RPA@PBE	251.480 (0.614)	**252.094**	252.035 (0.059)	251.813 (0.281)	252.031 (0.063)
MP2	289.988 (0.687)	**290.675**	290.368 (0.307)	290.108 (0.567)	290.458 (0.217)
Geometry optimization RPA@PBE					
RPA@PBE	255.243 (0.765)	**256.008**	255.095 (0.913)	254.795 (1.213)	255.328 (0.680)
MP2	292.923 (0.771)	**293.694**	292.847 (0.847)	292.486 (1.208)	293.112 (0.582)
(RPA+rSE)@PBE	304.317 (0.890)	**305.207**	304.513 (0.694)	304.202 (1.005)	304.843 (0.364)
Geometry optimization TTM2.1-F[a]					
RPA@PBE	252.065 (0.752)	**252.817**	252.437 (0.380)	252.264 (0.553)	252.513 (0.304)
MP2	286.984 (0.772)	**287.756**	287.197 (0.559)	287.024 (0.732)	287.308 (0.448)

[a]Ref[67]

4 Conclusion

We present an efficient sub-cubic implementation for RPA force calculations within the framework of AO basis sets and the LRI approximation. Such implementation allows us to

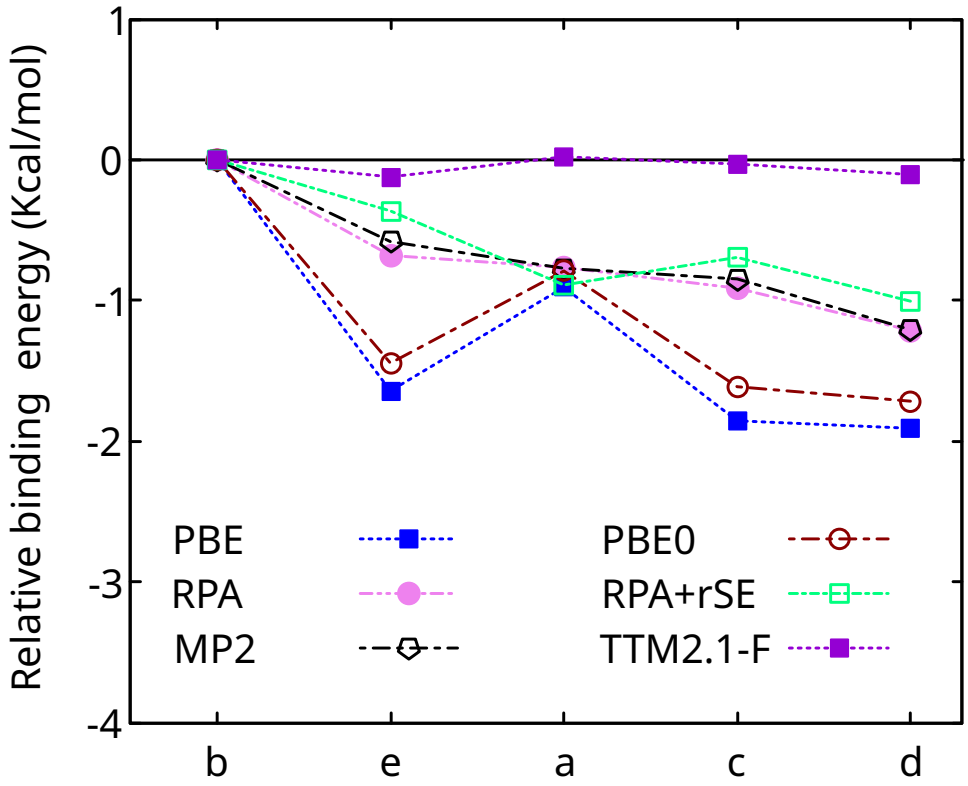

Figure 3: The relative binding energies (Kcal/mol) of the isomers of $(H_2O)_{25}$ with respect to isomer **b**, following the descending ordering of $b \rightarrow e \rightarrow a \rightarrow c \rightarrow d$, as given by RPA. For these calculations, the cc-pVQZ basis sets are used and the structure relaxation is performed for given methods, except for MP2 and (RPA+rSE)@PBE where RPA@PBE structures are used.

relax the structures of water clusters containing a few tens of water molecules using RPA at the level quadruple-ζ basis sets. Looking into the energy hierarchy of low-lying isomers of $(H_2O)_{21}$, $(H_2O)_{22}$, and $(H_2O)_{25}$ clusters using RPA and other methods reveals that the energy ordering pattern predicted by RPA is quite different from those yielded by the force field and GGA-PBE level of theories. In particular, in contrast with the water hexamer case, the energy hierarchy given by RPA with force-field, PBE or RPA geometries are also different for these larger water clusters. In general, the RPA energy ordering is much closer to the MP2 one compared to the force-field or GGA-PBE results, highlighting the importance of including non-local electron correlations in water cluster calculations. However, the RPA itself significantly underbinds the water clusters, and such underbinding becomes even more

pronounced at the CBS limit. This underbinding is well fixed by the rSE corrections, and in fact RPA+rSE yields binding energies that is on a par with the most accurate double hybrid functionals, at the CBS limit. The energy ordering of the low-lying isomers can be slightly different from RPA to RPA+rSE. In brief, RPA and its extensions provide a competitive class of approaches to study the structural and energetic properties of water clusters, as an alternative to traditional quantum chemistry approaches as MP2. However, their strong basis-set dependence needs to be addressed to make them computationally economic and practical.

Supporting Information Available

The following file is available free of charge.

- supporting_info.pdf: The file contains the following items:

    1. The structures of water cluster of size $n = 21, 22$ and 25, relaxed on the top of RPA@PBE using the QZ basis set and the frozen-core approximation.
    2. RPA@PBE, (RPA+rSE)@PBE, MP2, PBE, and PBE0 single point energies of the water monomer.

Acknowledgement

We acknowledge the funding support by the Strategic Priority Research Program of Chinese Academy of Sciences under Grant No. XDB0500201 and by the National Key Research and Development Program of China (Grant Nos. 2022YFA1403800 and 2023YFA1507004). This work was also supported by the Chinese National Science Foundation Grant Nos 12134012, 12374067, 12188101, 12274254, and T2222026. The numerical calculations in this study were partly carried out on the ORISE Supercomputer.

5 Supporting Information for "Efficient structural relaxation based on the random phase approximation: Applications to the water clusters "

5.1 Structures of the lowest-energy isomers of water clusters $(H_2O)_{21}$ relaxed using RPA@PBE with the cc-pVQZ basis set. The frozen-core approximation is used.

- a

0.30330010	−3.43960684	−4.13185228	O
1.22225508	−3.13289613	−3.99754878	H
−0.03162000	−3.57525289	−3.23335265	H
2.82912379	−5.29402016	1.04512867	O
2.45009851	−6.17233661	0.87374763	H
3.65047143	−5.28721399	0.51056961	H
−0.36878557	−3.94711550	−1.37155932	O
−1.24845807	−3.81536373	−1.00516285	H
0.25530550	−3.56353046	−0.71524376	H
1.56286253	−3.14213957	0.33484260	O
2.01256300	−3.98974291	0.62303442	H
1.38490627	−2.66407453	1.15147586	H
3.56226997	−8.97897038	−1.33714848	O
4.46317747	−8.58872834	−1.37113943	H
3.29215230	−9.10782219	−2.25990642	H
0.87752183	−6.34068734	−1.91859211	O
0.33596991	−5.57479678	−1.66077015	H
1.05242097	−6.85616653	−1.10655616	H
5.09308644	−7.77819749	−1.29825387	O

6.41828236	−7.56099626	−2.14181146	H
6.85550779	−6.71526543	−3.81812614	O
6.73331315	−5.73403237	−3.75984876	H
7.68810864	−6.84137090	−4.28247120	H
4.32018865	−7.11110623	−4.67315797	O
3.94128758	−7.99874581	−4.53947481	H
5.27011470	−7.14815620	−4.45266043	H
4.68759686	−3.19452770	−5.76722906	O
4.19714486	−3.97539427	−6.14225615	H
4.98484052	−2.67746709	−6.52120699	H
2.94680863	−2.93281449	−3.66063871	O
3.51322762	−2.78790653	−4.43741958	H
3.11451885	−3.87012874	−3.41148458	H
0.65952368	−5.40976051	−5.85941371	O
0.00887590	−5.28782862	−6.55807222	H
0.46429116	−4.69713844	−5.19784287	H
2.76447894	−9.23681254	−4.05188983	O
1.92637763	−8.72261088	−4.19888206	H
2.62167599	−10.10122827	−4.44788997	H
5.94295352	−2.81647432	−1.30872808	O
6.59829034	−2.23462947	−0.91344809	H
5.06865437	−2.35455987	−1.21510484	H
1.82505107	−7.76884230	0.16400706	O
1.42022446	−8.44853284	0.71055365	H
2.51480417	−8.24389142	−0.38434145	H
6.43881396	−4.10815299	−3.76351101	O
6.25429635	−3.59828378	−2.95767600	H

5.86285168	−3.74669461	−4.45763465	H
3.27158234	−5.45338382	−2.82675717	O
2.41337865	−5.80702408	−2.51614383	H
3.61785795	−6.09188329	−3.48548852	H
3.38563102	−5.32994885	−6.55280008	O
2.43110588	−5.30925583	−6.36538419	H
3.72725360	−6.03960380	−5.97904855	H
3.52774362	−1.76887844	−1.25466171	O
2.88497139	−2.19837778	−0.66758492	H
3.26738598	−2.06613279	−2.14868050	H
4.91324149	−5.30040138	−0.69614123	O
5.41075805	−4.46904281	−0.77519343	H
4.35495903	−5.33255325	−1.50393100	H
0.62428815	−7.73536134	−4.27795593	O
0.58013199	−7.27500067	−3.42030563	H
0.62692279	−7.00931027	−4.92531991	H

- **b**

0.34993576	−6.27070293	1.49782220	O
−0.05873985	−6.50224046	0.64564284	H
−0.03222052	−5.40025962	1.70732970	H
−1.41606633	−0.20862155	−1.90690594	O
−0.54594755	0.15290533	−2.14738370	H
−1.35555767	−1.14088903	−2.19886890	H
1.23578574	0.38588841	−2.59906298	O
1.54904125	1.13619610	−3.11270457	H
1.57987899	−0.42579256	−3.07408045	H
2.24529422	−1.72115237	−3.70820962	O
2.99020190	−2.06649595	−3.16985309	H
1.71731409	−2.49470867	−3.96272909	H
3.32082224	−3.05068877	2.22544724	O
2.52051825	−2.72004714	2.66407755	H
3.15650905	−3.98851208	2.02667212	H
4.25853514	−2.68524540	−2.14863961	O
4.43725646	−2.18222046	−1.34008727	H
3.86664250	−3.50855251	−1.80502470	H
0.82129156	−2.91846892	−0.41318180	O
1.20214120	−2.02445708	−0.28267427	H
0.36805872	−3.14983757	0.42206024	H
−0.99842724	−2.84725089	−2.38933595	O
−0.27798275	−2.89721433	−1.72239533	H
−0.59591775	−3.17544386	−3.21327202	H
2.72416913	−4.72436752	−1.06661552	O

2.98067469	−5.18920974	−0.25329331	H
2.05531857	−4.07138282	−0.76727690	H
0.23731616	0.07214340	1.99675016	O
−0.64192722	0.00583756	1.58846239	H
0.85106783	0.01803250	1.23857213	H
2.92294903	−5.73256277	1.50666608	O
3.41771305	−6.43169700	1.94363211	H
1.97237886	−6.02137586	1.51641801	H
4.34854715	−1.40529678	0.42913437	O
4.00552504	−2.05520400	1.09330512	H
5.10253542	−0.98295738	0.85114508	H
−2.63919908	−4.54475729	−1.02118282	O
−2.14105728	−3.93155352	−1.59859530	H
−2.85812939	−4.00689675	−0.24687990	H
−2.20527616	−0.20665553	0.56424781	O
−2.81908817	0.53334232	0.61868882	H
−1.87411879	−0.18770532	−0.38218033	H
−0.99019687	−6.62275577	−0.95388677	O
−1.52172546	−7.41271820	−1.09475320	H
−1.64094077	−5.87696596	−0.92603644	H
−2.97386483	−2.72274767	1.21930679	O
−3.76897946	−2.70835114	1.76075412	H
−2.80186140	−1.78720675	0.97124032	H
0.97670490	−1.98796654	3.43212131	O
0.99781354	−1.77254403	4.36903195	H
0.68513639	−1.16019576	2.96153551	H
0.56704787	−3.91188103	−4.36122133	O

0.74622757	−4.74746576	−3.85098923	H
0.46553373	−4.17666897	−5.27978586	H
1.87748663	−0.44423553	−0.11542272	O
2.82945600	−0.60973770	0.02224892	H
1.77454926	−0.01932973	−0.98923713	H
−0.47366364	−3.65606243	1.86412181	O
−1.39350400	−3.34874231	1.77881238	H
−0.07102303	−3.13063256	2.58024923	H
1.04795904	−5.99049080	−2.83214040	O
1.71850380	−5.65260057	−2.20651579	H
0.30622418	−6.24833925	−2.25967842	H

5.2 Structures of the lowest-energy isomers of water clusters $(H_2O)_{22}$ relaxed using RPA@PBE with the cc-pVQZ basis set. The frozen-core approximation is used.

- **a**

−0.70068807	2.38062258	−1.42309541	O
−0.55020091	2.94707208	−0.64724220	H
−2.39495380	0.07236942	3.90276973	H
3.76140342	2.28346572	2.68853460	O
0.06636984	1.77600306	−1.41096498	H
−2.25131829	0.80562113	2.55215216	H
1.40655769	1.55687541	1.59417549	O
4.06459735	2.96284120	2.05906016	H
−0.39684418	−0.22068607	3.21774153	H
−2.86422877	1.02708671	−0.80930951	O
4.21264622	1.45958960	2.42157821	H
0.54225190	0.52459815	4.16154068	H
−2.62263698	2.25269454	1.64831314	O
1.07834167	0.90792978	2.26015025	H
5.27523325	−0.64187751	1.72828962	H
1.45940017	0.70328096	−0.94341644	O
2.26206304	1.86927474	1.95405450	H
3.72229501	−0.65963074	1.67547445	H
−1.85486591	−1.28475681	0.45871043	O
−3.53030305	1.09020487	−1.50011992	H
1.95574136	2.66106451	5.32461509	H

1.69579840	5.33150376	1.23718862	O
−2.06936550	1.52368000	−1.14485452	H
3.11660740	2.79960286	4.31140479	H
4.05551554	3.92180072	0.50946051	O
−1.84013952	2.79000382	1.43197858	H
−2.43957812	3.72227077	4.23008532	H
0.63591022	−1.86069768	−0.25157749	O
−2.91840179	1.90478647	0.78753227	H
−3.35595120	2.93186019	3.32491934	H
−0.63380421	4.04419951	3.81213271	O
1.23445348	−0.24232386	−0.94360835	H
−2.87328380	1.82050102	5.16692197	H
−2.09863929	−0.06019410	2.98712119	O
1.44740613	0.93706230	0.01037687	H
−3.09363493	0.77230101	6.29492775	H
0.55759821	−0.12476428	3.42711493	O
−2.03509724	−1.07058546	1.38715255	H
−0.12835481	2.62320403	4.68589362	H
4.51786922	−0.07521177	1.55256886	O
−2.25563590	−0.55344244	−0.04190137	H
−0.61967306	1.53863180	5.65415499	H
2.69005880	3.23944856	5.06738651	O
1.83048200	5.48090358	2.18777174	H
4.34105643	0.93995579	−0.04002415	H
−3.25588781	3.19465225	4.25369354	O
2.50765940	4.89345303	0.93111738	H
3.20398032	1.26109049	−1.00632609	H

−2.50513663	0.99358538	5.56674838	O
4.77504975	4.45469835	0.15669941	H
0.35914210	2.77297227	1.31656155	H
0.18782402	1.86900191	5.22934010	O
4.04280854	3.09638699	−0.04387112	H
0.38675755	4.28867342	1.06795362	H
4.07725310	1.58444619	−0.71781107	O
0.58631567	−2.70818394	−0.70448673	H
1.80204358	−1.19787393	2.59245748	H
−0.24718034	3.53381805	1.13773062	O
−0.29386868	−1.66372881	0.02737669	H
1.83079331	−1.75594592	1.16697233	H
2.40161961	−1.59374711	1.93792175	O
−0.53420656	3.87232996	2.85465258	H
2.12750709	4.69836743	4.50026460	H
1.69934903	5.48756761	4.07847915	O
0.04326704	4.71905810	3.99729077	H
1.94570433	6.24353721	4.61974265	H

- **b**

−3.43475339	1.01487758	0.65012457	O
−4.01884491	1.62825679	0.19466910	H
−1.75065503	−6.00283767	−1.53895892	H
−2.45900997	0.15169806	6.04960907	O
−3.86208525	0.12285209	0.57800131	H
−1.38872105	−5.60105189	−0.07440169	H
−0.22331526	−0.36405295	2.80510715	O
−2.64541626	0.49605072	5.16078214	H
−0.54649594	−6.02972714	1.93807146	H
−2.76914825	0.43207726	3.26954714	O
−1.51970297	−0.09022743	6.00746433	H
−1.94098043	−5.39481946	2.02295064	H
2.49182483	−2.20757833	5.11522919	O
−0.11511962	−0.61925678	3.74900763	H
2.32197834	−2.20717453	2.01772269	H
−3.80493459	−2.15079470	6.21193154	O
−0.39975552	−1.20565323	2.32422214	H
1.68840452	−0.89055510	2.50530732	H
−0.03983333	−1.12188163	5.36026843	O
−1.84493758	0.19270901	3.04330067	H
−1.11530057	−2.64190409	0.63688088	H
1.05858623	−4.64284212	5.07522288	O
−3.10231224	0.88260800	2.47629450	H
0.25680485	−3.05402402	1.32822665	H
−4.14405038	−1.90790665	3.40242969	O

2.58549479	−1.91972612	4.17068712	H
−3.04638768	−3.20756517	3.03405102	H
−0.67049761	0.67355711	0.21501087	O
3.34693218	−2.05034601	5.52639689	H
−1.64268811	−3.37727264	2.40854192	H
1.11100487	−5.85105927	2.72884953	O
−3.35695124	−1.26901752	6.24524736	H
1.70549898	−4.57463173	1.60415043	H
−1.39704320	−5.27699229	−1.01635858	O
−4.38692362	−2.17667050	6.97741916	H
1.65507050	−3.83993869	0.20080810	H
−1.41220008	−6.01783982	1.49406708	O
−0.52359224	−1.97858215	5.38673072	H
0.61448379	−2.85698205	−1.50110169	H
2.48875503	−1.43218822	2.58442584	O
0.89248813	−1.36274967	5.49525401	H
0.19988299	−4.33675288	−1.40094051	H
−0.57557535	−2.54615031	1.44768866	O
1.62347438	−3.85325138	5.13133212	H
−0.12341862	−0.70275024	−2.44944499	H
−2.31660192	−3.85516541	2.94064074	O
0.18664717	−4.34842156	5.38479329	H
−0.38428624	−0.51040292	−0.93497555	H
1.78342966	−3.70846861	1.16595695	O
−3.64378899	−1.06257433	3.38878561	H
−2.14526883	−3.68112889	−0.87733347	H
0.97479959	−3.75146186	−1.38561734	O

−4.32969613	−2.05591919	4.34323209	H
−1.77948634	−2.20695777	−1.22619928	H
−0.31969448	−1.19564541	−1.64664258	O
−0.36307158	0.51100965	1.11862677	H
−2.24644435	−3.19149337	5.91395559	H
−2.27572201	−2.75594700	−0.59288308	O
−1.62119140	0.85976875	0.30844587	H
−1.74270616	−3.64155727	4.52919211	H
−1.43304157	−3.43189167	5.44033864	O
1.07540130	−5.40679738	3.61611632	H
−3.73294881	−2.01533666	0.20918536	H
−4.41389514	−1.44501626	0.60668968	O
1.58244577	−6.67584686	2.88366347	H
−4.53287077	−1.76594450	1.51328853	H

5.3 Structures of the lowest-energy isomers of water clusters $(H_2O)_{25}$ relaxed using RPA@PBE with the cc-pVQZ basis set. The frozen-core approximation is used.

- **a**

10.40603729	10.50814590	−11.06728442	*O*
9.58139714	10.44801855	−10.57546758	*H*
11.08742465	10.79333906	−10.40549403	*H*
14.75502692	10.48409184	−12.78323102	*O*
14.48391170	9.70124746	−12.25338033	*H*
15.67459675	10.71926659	−12.52603249	*H*
17.14332144	13.25734889	−13.95020001	*O*
16.30435185	13.68485487	−14.18012014	*H*
17.40442686	12.78937782	−14.76132496	*H*
15.91800664	7.05328070	−12.87002876	*O*
15.77809381	7.09203071	−13.83043498	*H*
16.68356617	7.63198772	−12.72083906	*H*
11.00626268	12.06499279	−13.26054163	*O*
10.64916381	11.62529900	−12.46838517	*H*
11.90361099	12.37313862	−13.00169070	*H*
12.34412207	14.99685959	−16.22855824	*O*
12.08417210	15.90706430	−16.39855216	*H*
11.53327528	14.54647182	−15.87782397	*H*
14.95816247	11.89332138	−16.62514823	*O*
15.92781259	11.81616403	−16.67198344	*H*
14.65745102	11.08222713	−16.15730282	*H*

14.43998670	9.51332838	−9.27655457	O
14.54305256	8.88877237	−8.55205770	H
14.26466454	8.96448495	−10.07623070	H
13.51019105	12.80551360	−12.65752705	O
13.86897616	13.24310316	−13.46429984	H
13.93802843	11.91778394	−12.65696220	H
14.09085762	9.77304891	−15.23469916	O
14.39996512	10.03909579	−14.33760829	H
13.11046705	9.85959766	−15.18503044	H
18.06131826	8.93054391	−12.65668567	O
17.80697157	9.84153645	−12.37947013	H
18.90525085	8.75647021	−12.22882035	H
12.26211696	11.27559883	−9.35220192	O
12.98818893	10.63755253	−9.24276396	H
12.70649790	12.11935814	−9.53877985	H
10.64611337	11.46866026	−17.27797446	O
10.13311293	11.21017968	−18.04931293	H
11.45454676	11.92106994	−17.63167881	H
14.50149402	13.90127112	−14.87507013	O
13.81742618	14.45701003	−15.28779918	H
14.64043717	13.17227406	−15.51986719	H
17.67713889	11.66246016	−16.24092153	O
17.77648621	10.71851959	−15.95331882	H
18.39162795	11.81562065	−16.86668045	H
13.81961982	13.49264317	−10.12461212	O
13.72223822	13.39884052	−11.10210579	H
13.70834378	14.42748799	−9.92924557	H

17.88598701	9.15285873	−15.44492856	O
18.03540175	9.05246377	−14.48896679	H
17.13136559	8.57095664	−15.63507921	H
16.06983340	11.82384876	−9.68725608	O
15.36941940	12.49393104	−9.74944003	H
15.59174644	11.00253592	−9.48694949	H
11.45085923	10.06731113	−15.02539989	O
11.09822896	10.38575297	−15.87475021	H
11.29232424	10.81280477	−14.40441856	H
15.54244057	7.59974472	−15.62663577	O
14.88365911	8.33214501	−15.56845587	H
15.23774179	7.01565108	−16.32697864	H
12.78450433	12.83619696	−18.04971691	O
12.68924010	13.68804835	−17.59348849	H
13.61767156	12.47431751	−17.69849816	H
11.50919851	8.43283713	−12.66473048	O
11.04057133	9.07576121	−12.10602714	H
11.42146059	8.78739987	−13.56255729	H
17.15503337	11.34230402	−12.07397859	O
16.85364021	11.63537240	−11.18353537	H
17.18414824	12.12106823	−12.67404248	H
10.23386876	13.60553492	−15.42244068	O
10.16740327	12.89002648	−16.07551067	H
10.38144838	13.14042492	−14.57960727	H
13.94750426	8.28127286	−11.56049727	O
14.58422771	7.70597935	−12.04344566	H
13.06756066	8.22014347	−11.99565773	H

- **b**

16.48813723	9.97857548	−15.02009849	O
17.29457224	9.41238436	−15.03162479	H
15.74584600	9.41821795	−15.34753980	H
14.81995857	7.33481810	−9.23963843	O
14.98276256	6.74452220	−8.49845169	H
15.19905444	8.21819828	−8.98103934	H
17.02625312	12.54166449	−15.32139621	O
16.95464994	12.84940679	−16.22959082	H
16.77785398	11.58735162	−15.33541663	H
12.43661267	8.47626339	−10.25611071	O
13.15220846	7.94576691	−9.86958896	H
12.69550130	9.39615277	−10.07377778	H
14.41950136	8.48234425	−15.71943579	O
14.68179853	7.93301128	−16.47916679	H
14.26541427	7.83647835	−14.99457939	H
18.65783175	8.45662114	−14.88786955	O
19.40582953	9.00501180	−14.58623292	H
18.44548613	7.86647427	−14.12886729	H
20.51754786	10.08254678	−13.70642456	O
20.09142885	10.97889943	−13.70023031	H
21.43068992	10.23271027	−13.96892703	H
18.07594512	6.73527958	−12.90949342	O
17.97270565	5.90253222	−13.40354206	H
17.20973784	6.88319298	−12.47480825	H
11.67892799	8.02962239	−12.74998343	O

11.95553575	8.19075211	−11.81206091	H
10.76623384	7.72980107	−12.69618742	H
15.63613519	13.43742875	−13.02738759	O
16.05907892	13.24810967	−13.88106945	H
16.34936968	13.30674507	−12.38056427	H
12.55544848	10.20806343	−14.36056003	O
13.12387478	9.75065505	−14.99909076	H
12.15178627	9.48584271	−13.84999352	H
13.77719685	11.62443758	−12.43136491	O
13.30016530	11.24653841	−13.20284289	H
14.36308903	12.35716435	−12.73200118	H
13.42313453	11.07461635	−9.87788437	O
13.50164829	11.36391639	−10.81730553	H
12.91173726	11.76084766	−9.43853089	H
17.60968249	4.64369705	−14.68221349	O
16.63883490	4.63824297	−14.88427955	H
17.86025169	3.71932790	−14.59225138	H
15.66662687	7.29130822	−11.83574764	O
15.62285926	8.26263035	−11.99572213	H
15.43552812	7.16804937	−10.89681581	H
18.05204939	6.51862769	−16.78356630	O
18.07191581	5.77962397	−16.15334461	H
18.38346123	7.26916471	−16.25993530	H
17.87397212	12.86606480	−11.33924770	O
18.15176788	13.41447843	−10.59940646	H
17.84944093	11.93896619	−10.99545232	H
15.49958237	6.65887115	−17.49805712	O

16.47121433	6.66194886	−17.30177999	H
15.42547428	6.55407920	−18.45115622	H
15.74084827	9.83737064	−12.47564792	O
16.05217293	9.91373942	−13.40587872	H
14.98464713	10.46134869	−12.40899667	H
19.32783805	12.43844438	−13.69688555	O
18.61112339	12.53255521	−14.34656900	H
18.91185610	12.66499822	−12.84710755	H
17.63375347	10.30951785	−10.67624120	O
16.97845419	10.12768784	−11.38650742	H
18.37949413	9.69823028	−10.87094606	H
13.87830520	6.70405207	−13.74975692	O
14.49320953	6.85168972	−12.99886519	H
13.01252131	7.00854271	−13.42294098	H
19.61568964	8.63105576	−11.42408494	O
19.23597271	7.83886866	−11.83586478	H
20.05667064	9.09551115	−12.15421489	H
15.69603871	9.76415803	−8.78518552	O
16.46541002	9.95947751	−9.35420673	H
14.98874032	10.34523289	−9.11002237	H
15.05116506	4.79667362	−15.37544579	O
15.06446450	5.30793494	−16.20067951	H
14.52457582	5.34606185	−14.76783907	H

- **c**

−7.84140253	−2.13833377	6.07704888	O
−6.93153680	−1.83820632	6.23802889	H
−8.42831064	−1.42271275	6.37063302	H
−10.26801852	−2.41923132	2.37942217	O
−9.63842094	−2.99514610	2.83964750	H
−10.38244148	−1.68724071	3.01245620	H
−8.20984207	−3.64779813	3.94180857	O
−8.11676787	−3.08214176	4.74956874	H
−8.19359367	−4.55379117	4.26418975	H
−5.52297367	0.66705417	0.32717203	O
−5.82036399	−0.20423908	0.01055106	H
−6.33745352	1.08020585	0.68765270	H
−6.39165797	1.08755997	5.66884120	O
−6.76801415	0.63515886	4.87823174	H
−5.88820858	0.39014255	6.12279120	H
−5.15951761	5.10965726	1.00445353	O
−5.23579392	5.85600524	0.40251079	H
−4.86328540	4.34559010	0.44632124	H
−10.13966271	1.58238516	0.49995265	O
−10.65519001	2.03123724	−0.17574917	H
−10.55237468	1.81629139	1.37729934	H
−9.72645789	−0.14611092	6.76674329	O
−10.29699339	−0.23349878	7.53559440	H
−9.42972647	0.79970129	6.74765297	H
−4.15485580	−1.50638747	3.96145735	O

−3.92535455	−0.68140061	3.49842381	H
−4.86810906	−1.87826311	3.41237907	H
−4.19804636	3.03099796	−0.34030993	O
−3.34494555	2.85880562	0.09007329	H
−4.67113657	2.18250698	−0.28466578	H
−10.07511676	−0.21674397	4.04062692	O
−9.10677318	−0.17829176	3.87801515	H
−10.15405972	−0.26984444	5.00795266	H
−6.77219247	−1.74224170	−0.14140135	O
−6.73602730	−2.32170710	−0.90820607	H
−7.73078010	−1.47180490	−0.05150937	H
−3.87753490	0.81526216	2.44905474	O
−4.45739095	0.67749418	1.66759341	H
−3.09372630	1.27775839	2.10598890	H
−7.45615599	0.02868439	3.47198015	O
−7.07673800	−0.79757065	3.10583397	H
−7.54180095	0.64319841	2.71353921	H
−5.18336270	−1.25944908	6.35638930	O
−4.72667465	−1.36172289	5.47709693	H
−4.57459651	−1.60441908	7.01556225	H
−2.03982546	2.64647231	1.46303288	O
−1.07994241	2.69286166	1.43477380	H
−2.33612221	3.37884511	2.05891950	H
−9.19386157	3.93355691	4.22790270	O
−9.46863763	4.81710656	4.49384642	H

−8.36594712	4.06685706	3.71985687	H
−10.95714191	2.10529553	2.92113036	O
−10.70905294	1.28146654	3.38996164	H
−10.41154587	2.79065888	3.33901006	H
−6.38413371	−2.25080930	2.51681354	O
−6.99305244	−2.91824828	2.88539959	H
−6.49012062	−2.25408943	1.54791623	H
−9.25663082	−1.11723776	0.23166429	O
−9.63855094	−1.60553470	0.99487590	H
−9.61330730	−0.21788412	0.28870937	H
−8.69294618	2.27277857	6.54712575	O
−8.92767462	2.83039515	5.78873499	H
−7.80107544	1.94005147	6.32988751	H
−3.16693800	4.51898755	2.99119271	O
−3.79823816	4.93443541	2.38211883	H
−3.73125910	4.00666473	3.59533428	H
−4.98171833	2.68631866	4.04572542	O
−5.40364777	2.17576386	4.76828004	H
−4.62244433	1.99212778	3.44954234	H
−7.65002602	1.77855785	1.47357284	O
−7.45909348	2.64740760	1.88872014	H
−8.51473390	1.83650838	1.02495085	H
−6.91073647	3.97214175	2.77970279	O
−6.19020458	3.51145856	3.28100093	H
−6.43433146	4.52962255	2.13784168	H

- **d**

10.47809957	12.71846274	−11.97899901	O
10.22658342	11.89488486	−11.52970077	H
10.63625709	12.49532394	−12.91029371	H
14.09311777	9.12486699	−17.83882468	O
14.26174373	8.51196398	−18.56013848	H
13.10630803	9.20798153	−17.77040535	H
11.69453872	9.05046944	−12.03404201	O
12.36811207	9.70239422	−11.73499234	H
10.88336492	9.32340836	−11.57297533	H
14.62855857	9.10960050	−15.14736265	O
15.04774856	9.99768970	−15.03923400	H
14.56493375	8.97001955	−16.11036183	H
13.32650857	12.38957845	−9.32295825	O
12.90076051	13.20379791	−9.65514210	H
14.19725408	12.62292269	−8.95504684	H
14.43476965	11.93385919	−17.40490086	O
14.94282447	11.94997045	−16.57508141	H
14.49004863	11.01159577	−17.70012802	H
11.93221506	9.46054541	−14.67181434	O
12.89870640	9.36433235	−14.77818760	H
11.75816995	9.22359852	−13.73655079	H
13.68652459	8.31293402	−8.87335154	O
13.67033485	7.85216735	−9.75079694	H
13.67255193	7.60370134	−8.22239526	H
13.63683144	10.74820678	−11.40476492	O

14.56221812	10.44172678	−11.49171232	H
13.60096143	11.34194525	−10.62443672	H
11.70118834	10.28785052	−8.59490226	O
12.32392522	9.54731504	−8.70030405	H
12.25965659	11.07677455	−8.71232606	H
16.61741640	13.54203067	−11.14983835	O
15.81349085	14.04490669	−11.40797636	H
16.43050485	13.18561540	−10.26683097	H
9.87985870	10.38924823	−10.48691704	O
9.00248313	10.24051141	−10.12259110	H
10.50869353	10.34382583	−9.71743547	H
13.62492826	12.52626433	−13.39178907	O
12.76367580	12.44578183	−13.85300840	H
13.57364288	11.88608854	−12.64794357	H
16.13883173	9.81173163	−11.73868728	O
16.73224890	10.43103936	−12.20556120	H
16.08795271	8.99566520	−12.26703525	H
15.52426847	7.56884827	−13.18783620	O
15.20780246	8.02398796	−14.00378175	H
16.10322154	6.86075037	−13.48563599	H
14.39098362	14.78594157	−12.05049633	O
14.08762084	14.06646642	−12.63558853	H
13.62496120	14.91209799	−11.47230151	H
13.47332430	7.11773242	−11.22943415	O
12.73455972	7.64766434	−11.58197315	H

14.16968424	7.19162291	−11.90028752	H
17.49712477	11.85293197	−12.90949885	O
17.17398081	12.53221290	−12.24768878	H
18.44525267	11.99645319	−12.98317492	H
11.27167404	12.06655647	−14.59614680	O
11.30210752	12.37717355	−15.51650851	H
11.46875076	11.10520456	−14.66550762	H
15.94176198	12.44968401	−8.62262091	O
16.41565701	12.70294167	−7.82525818	H
15.99909733	11.45857710	−8.67591215	H
15.57146298	11.57615800	−14.88087092	O
16.37366583	11.72493833	−14.35151506	H
14.84687749	11.96299904	−14.32863771	H
11.80450214	12.38394407	−17.30332256	O
11.57520664	13.07195211	−17.93516066	H
12.79058342	12.31404328	−17.33189525	H
16.02843534	9.85364647	−8.98165862	O
16.20377252	9.75353651	−9.93403619	H
15.21200427	9.34110670	−8.84457852	H
11.97249104	14.37757249	−10.55777948	O
11.42184672	13.78744725	−11.13159879	H
11.34642591	14.97802443	−10.14219663	H
11.51355405	9.54533398	−17.41872688	O
11.42251862	10.50999168	−17.49156768	H
11.42433060	9.37419908	−16.46557003	H

- **e**

−0.86725915	3.70975315	2.59411208	O
−0.40769972	2.93270089	2.96642655	H
−1.61634808	3.38449245	2.06079563	H
−2.80406051	5.79337884	−0.23995074	O
−1.92617019	5.80859896	−0.67984184	H
−2.74068262	6.47681739	0.45221079	H
4.26880190	6.67983351	0.63834423	O
5.00097865	7.27966323	0.46753456	H
3.85124988	6.51942855	−0.24285212	H
1.92201346	7.10472250	1.92433925	O
1.93151953	6.96883271	2.89113413	H
2.84415981	7.06371237	1.60796604	H
−0.38476086	5.60254337	−1.35791339	O
0.09173621	5.39813668	−0.51435600	H
−0.04099486	6.46239781	−1.66166820	H
2.62346955	3.17463001	−0.06723413	O
1.95861397	3.82852465	0.23798401	H
2.66995149	3.29121485	−1.02892376	H
0.78828302	4.91242216	0.86879847	O
0.20578115	4.46848620	1.52297577	H
1.20062830	5.67839359	1.32203236	H
−2.19956215	7.65150579	1.70672297	O
−1.80058942	7.13880137	2.46082298	H
−2.83780010	8.24390471	2.11673630	H
−0.94169003	1.77560140	−0.68117308	O

−0.58130708	2.31872433	−1.40917991	H
−1.52366250	2.38580977	−0.18452714	H
−1.17515246	6.21541086	3.64938347	O
−1.14091107	5.28069774	3.37441308	H
−0.29109810	6.37434169	4.02004746	H
−2.73546883	3.29211573	0.72653963	O
−3.57112994	2.87099158	0.46142005	H
−2.79845616	4.22141569	0.41013648	H
0.16002687	8.71450774	0.58503968	O
0.80230731	8.22544192	1.13368873	H
−0.70641938	8.42600994	0.92002094	H
1.21719477	1.00040500	0.87932802	O
1.83785519	1.65933366	0.51437079	H
0.40948010	1.16691730	0.35696529	H
−0.18838950	3.40145867	−2.79664881	O
−0.99431735	3.30092220	−3.33463186	H
−0.30547420	4.25795899	−2.32498647	H
0.76270178	8.00662289	−1.84659875	O
0.50780643	8.36671577	−0.95161071	H
0.58583428	8.70406355	−2.48391302	H
−3.15221354	0.85428930	−2.13654606	O
−3.03645373	1.44228223	−2.89980232	H
−2.32538662	0.98256979	−1.63322665	H
2.49580315	3.96667598	3.92605449	O
3.16925107	4.00701627	3.21309511	H

1.96179260	3.17696430	3.74399693	H
−4.29546743	4.46569054	−2.20249181	O
−4.69744863	3.77405343	−1.65213944	H
−3.87935213	5.06928359	−1.56392304	H
−2.71904527	3.10777008	−3.86936421	O
−3.28834527	3.67601034	−3.29153023	H
−3.01401926	3.28133968	−4.76847355	H
0.82519551	1.76005575	3.33676137	O
0.78615069	1.00215427	3.92693861	H
0.99380525	1.39423363	2.42115044	H
2.45505046	3.80091129	−2.80686555	O
1.52397300	3.56251471	−3.00386658	H
2.98199227	3.43177351	−3.52177597	H
1.51561874	6.30403677	4.45701685	O
1.85826197	5.37703866	4.30463279	H
1.85913931	6.57108215	5.31444017	H
4.32773512	4.11098255	1.91270714	O
4.47824235	5.00599992	1.57371018	H
3.89114039	3.67311373	1.16091911	H
−4.87224006	2.17896092	−0.61515456	O
−5.64563646	1.66633852	−0.36345059	H
−4.31487890	1.58455404	−1.18118414	H
3.03740748	6.36084721	−1.69058605	O
2.80026455	5.52007563	−2.11157256	H
2.28056829	6.95489723	−1.82084674	H

Table 5: The MP2, RPA@PBE, (RPA+rSE)@PBE, PBE0, and PBE single point energies for H_2O molecule. The structures are optimized for different levels of theory and basis set. For RPA@PBE and (RPA+rSE)@PBE the frozen-core approximation is used for structure relaxation and single point energy calculations.

H_2O	E (Hartree)
Own Geometries	
MP2[aTZ][a]	−76.328992
PBE[aTZ][b]	−76.380357
PBE[QZ][b]	−76.383283
PBE[light][b]	−76.383342
PBE[tight][b]	−76.388204
PBE0[QZ][b]	−76.383553
Geometry optimization RPA@PBE[QZ]	
RPA@PBE[QZ][b]	−76.497036
MP2[QZ][b]	−76.347596
(RPA+rSE)@PBE[QZ][b]	−76.505122
Geometry optimization PBE[QZ]	
RPA@PBE[QZ][b]	−76.496966
MP2[QZ][b]	−76.347420
Geometry used for TTM2.1-F with (R_{O-H}) 0.9578 Å, (θ) 104.51°	
RPA@PBE[QZ][b]	−76.496984
MP2[QZ][b]	−76.347643

[a]Ref 67 [b]This work (results obtained using FHI-aims)

References

(1) Ludwig, R. Water: From Clusters to the Bulk. *Angewandte Chemie International Edition* **2001**, *40*, 1808–1827.

(2) Brini, E.; Fennell, C. J.; Fernandez-Serra, M.; Hribar-Lee, B.; Lukšič, M.; Dill, K. A. How Water's Properties Are Encoded in Its Molecular Structure and Energies. *Chemical Reviews* **2017**, *117*, 12385–12414, PMID: 28949513.

(3) Bulusu, S.; Yoo, S.; Aprà, E.; Xantheas, S.; Zeng, X. C. Lowest-Energy Structures of Water Clusters (H2O)11 and (H2O)13. *The Journal of Physical Chemistry A* **2006**, *110*, 11781–11784, PMID: 17048809.

(4) Jorgensen, W. L.; Chandrasekhar, J.; Madura, J. D.; Impey, R. W.; Klein, M. L.

Comparison of simple potential functions for simulating liquid water. *The Journal of Chemical Physics* **1983**, *79*, 926–935.

(5) Fanourgakis, G. S.; Xantheas, S. S. Development of transferable interaction potentials for water. V. Extension of the flexible, polarizable, Thole-type model potential (TTM3-F, v. 3.0) to describe the vibrational spectra of water clusters and liquid water. *The Journal of Chemical Physics* **2008**, *128*, 074506.

(6) Babin, V.; Medders, G. R.; Paesani, F. Toward a Universal Water Model: First Principles Simulations from the Dimer to the Liquid Phase. *The Journal of Physical Chemistry Letters* **2012**, *3*, 3765–3769, PMID: 26291108.

(7) Møller, C.; Plesset, M. S. Note on an Approximation Treatment for Many-Electron Systems. *Phys. Rev.* **1934**, *46*, 618–622.

(8) Santra, B.; Michaelides, A.; Scheffler, M. On the accuracy of density-functional theory exchange-correlation functionals for H bonds in small water clusters: Benchmarks approaching the complete basis set limit. *The Journal of Chemical Physics* **2007**, *127*, 184104.

(9) Santra, B.; Michaelides, A.; Fuchs, M.; Tkatchenko, A.; Filippi, C.; Scheffler, M. On the accuracy of density-functional theory exchange-correlation functionals for H bonds in small water clusters. II. The water hexamer and van der Waals interactions. *The Journal of Chemical Physics* **2008**, *129*, 194111.

(10) Bohm, D.; Pines, D. A Collective Description of Electron Interactins: III. Coulomb Interaction in a Degenerate Electron Gas. *Phys. Rev.* **1953**, *92*, 609.

(11) Furche, F. Molecular tests of the random phase approximation to the exchange-correlation energy functional. *Phys. Rev. B* **2001**, *64*, 195120.

(12) Ren, X.; Rinke, P.; Joas, C.; Scheffler, M. Random-phase approximation and its applications in computational chemistry and materials science. *J. Mater. Sci.* **2012**, *47*, 7447.

(13) Eshuis, H.; Bates, J. E.; Furche, F. Electron Correlation Methods Based on the Random Phase Approximation. *Theor. Chem. Acc.* **2012**, *131*, 1084.

(14) Heßelmann, A.; Görling, A. Random-phase approximation correlation methods for molecules and solids. *Mol. Phys.* **2011**, *109*, 2473.

(15) Langreth, D. C.; Perdew, J. P. Exchange-correlation energy of a metal surface: Wavevector analysis. *Phys. Rev. B* **1977**, *15*, 2884.

(16) Gunnarsson, O.; Lundqvist, B. I. Exchange and correlation in atoms, molecules, and solids by the spin-density-functional formalism. *Phys. Rev. B* **1976**, *13*, 4274.

(17) Perdew, J. P.; Schmidt, K. In *Density Functional Theory and its Application to Materials* ; Van Doren, V., Van Alsenoy, C., Geerlings, P., Eds.; AIP: Melville, NY, 2001.

(18) Dobson, J. F.; Wang, J.; Dinte, B. P.; McLennan, K.; Le, H. M. Soft cohesive forces. *International Journal of Quantum Chemistry* **2005**, *101*, 579–598.

(19) Dobson, J. F.; Gould, T. Calculation of dispersion energies. *J. Phys.: Condens. Matter* **2012**, *24*, 073201.

(20) Toulouse, J.; Gerber, I. C.; Jansen, G.; Savin, A.; Ángyán, J. G. Adiabatic-Connection Fluctuation-Dissipation Density-Functional Theory Based on Range Separation. *Phys. Rev. Lett.* **2009**, *102*, 096404.

(21) Zhu, W.; Toulouse, J.; Savin, A.; Ángyán, J. G. Range-separated density-functional theory with random phase approximation applied to noncovalent intermolecular interactions. *J. Chem. Phys.* **2010**, *132*, 244108.

(22) Heßelmann, A.; Görling, A. Correct Description of the Bond Dissociation Limit without Breaking Spin Symmetry by a Random-Phase-Approximation Correlation Functional. *Phys. Rev. Lett.* **2011**, *106*, 093001.

(23) Ren, X.; Tkatchenko, A.; Rinke, P.; Scheffler, M. Beyond the Random Phase Approximation for the Electron Correlation Energy: The Importance of Single Excitations. *Phys. Rev. Lett.* **2011**, *106*, 153003.

(24) Eshuis, H.; Furche, F. A Parameter-Free Density Functional That Works for Noncovalent Interactions. *J. Phys. Chem. Lett.* **2011**, *2*, 983.

(25) Ren, X.; Rinke, P.; Scuseria, G. E.; Scheffler, M. Renormalized second-order perturbation theory for the electron correlation energy: Concept, implementation, and benchmarks. *Phys. Rev. B* **2013**, *88*, 035120.

(26) Ren, X.; Rinke, P.; Scheffler, M. Exploring the random phase approximation: Application to CO adsorbed on Cu(111). *Phys. Rev. B* **2009**, *80*, 045402.

(27) Schimka, L.; Harl, J.; Stroppa, A.; Grüneis, A.; Marsman, M.; Mittendorfer, F.; Kresse, G. Accurate surface and adsorption energies from many-body perturbation theory. *Nature Materials* **2010**, *9*, 741.

(28) Lebègue, S.; Harl, J.; Gould, T.; Ángyán, J. G.; Kresse, G.; Dobson, J. F. Cohesive Properties and Asymptotics of the Dispersion Interaction in Graphite by the Random Phase Approximation. *Phys. Rev. Lett.* **2010**, *105*, 196401.

(29) Zhang, M.-Y.; Cui, Z.-H.; Jiang, H. Relative stability of FeS_2 polymorphs with the random phase approximation approach. *J. Mater. Chem. A* **2018**, *6*, 6606–6616.

(30) Sengupta, N.; Bates, J. E.; Ruzsinszky, A. From semilocal density functionals to random phase approximation renormalized perturbation theory: A methodological assessment of structural phase transitions. *Phys. Rev. B* **2018**, *97*, 235136.

(31) Cazorla, C.; Gould, T. Polymorphism of bulk boron nitride. *Science Advances* **2019**, *5*, eaau5832.

(32) Yang, S.; Ren, X. Phase stability of the argon crystal: first-principles study based on random phase approximation plus renormalized single excitation corrections. *New J. Phys.* **2022**, *24*, 033049.

(33) Dobson, J. F. In *Topics in Condensed Matter Physics*; Das, M. P., Ed.; Nova: New York, 1994.

(34) Chedid, J.; Jocelyn, N.; Eshuis, H. Energies, structures, and harmonic frequencies of small water clusters from the direct random phase approximation. *The Journal of Chemical Physics* **2021**, *155*, 084303.

(35) Tahir, M. N.; Zhu, T.; Shang, H.; Li, J.; Blum, V.; Ren, X. Localized Resolution of Identity Approach to the Analytical Gradients of Random-Phase Approximation Ground-State Energy: Algorithm and Benchmarks. *Journal of Chemical Theory and Computation* **2022**, *18*, 5297–5311, PMID: 35959556.

(36) Del Ben, M.; Hutter, J.; VandeVondele, J. Probing the structural and dynamical properties of liquid water with models including non-local electron correlation. *The Journal of Chemical Physics* **2015**, *143*, 054506.

(37) Yao, Y.; Kanai, Y. Nuclear Quantum Effect and Its Temperature Dependence in Liquid Water from Random Phase Approximation via Artificial Neural Network. *The Journal of Physical Chemistry Letters* **2021**, *12*, 6354–6362, PMID: 34231366.

(38) Macher, M.; Klimeš, J.; Franchini, C.; Kresse, G. The random phase approximation applied to ice. *The Journal of Chemical Physics* **2014**, *140*, 084502.

(39) Rekkedal, J.; Coriani, S.; Iozzi, M. F.; Teale, A. M.; Helgaker, T.; Pedersen, T. B.

Communication: Analytic gradients in the random-phase approximation. *The Journal of Chemical Physics* **2013**, *139*, 081101.

(40) Mussard, B.; Szalay, P. G.; Ángyán, J. G. Analytical Energy Gradients in Range-Separated Hybrid Density Functional Theory with Random Phase Approximation. *Journal of Chemical Theory and Computation* **2014**, *10*, 1968–1979, PMID: 26580524.

(41) Burow, A. M.; Bates, J. E.; Furche, F.; Eshuis, H. Analytical First-Order Molecular Properties and Forces within the Adiabatic Connection Random Phase Approximation. *Journal of Chemical Theory and Computation* **2014**, *10*, 180–194, PMID: 26579901.

(42) Ramberger, B.; Schäfer, T.; Kresse, G. Analytic Interatomic Forces in the Random Phase Approximation. *Phys. Rev. Lett.* **2017**, *118*, 106403.

(43) Rojas, H. N.; Godby, R. W.; Needs, R. J. Space-Time Method for *Ab Initio* Calculations of Self-Energies and Dielectric Response Functions of Solids. *Phys. Rev. Lett.* **1995**, *74*, 1827.

(44) Liu, P.; Kaltak, M.; Klimeš, J.; Kresse, G. Cubic scaling GW: Towards fast quasiparticle calculations. *Phys. Rev. B* **2016**, *94*, 165109.

(45) Beuerle, M.; Ochsenfeld, C. Low-scaling analytical gradients for the direct random phase approximation using an atomic orbital formalism. *J. Chem. Phys.* **2018**, *149*, 244111.

(46) Ihrig, A. C.; Wieferink, J.; Zhang, I. Y.; Ropo, M.; Ren, X.; Rinke, P.; Scheffler, M.; Blum, V. Accurate localized resolution of identity approach for linear-scaling hybrid density functionals and for many-body perturbation theory. *New Journal of Physics* **2015**, *17*, 093020.

(47) Mezei, P. D.; Csonka, G. I.; Ruzsinszky, A.; Kállay, M. Construction and Application

of a New Dual-Hybrid Random Phase Approximation. *Journal of Chemical Theory and Computation* **2015**, *11*, 4615–4626, PMID: 26574252.

(48) Mezei, P. D.; Ruzsinszky, A.; Csonka, G. I. Application of a Dual-Hybrid Direct Random Phase Approximation to Water Clusters. *Journal of Chemical Theory and Computation* **2016**, *12*, 4222–4232, PMID: 27500940.

(49) Bryantsev, V. S.; Diallo, M. S.; van Duin, A. C. T.; Goddard, W. A. I. Evaluation of B3LYP, X3LYP, and M06-Class Density Functionals for Predicting the Binding Energies of Neutral, Protonated, and Deprotonated Water Clusters. *Journal of Chemical Theory and Computation* **2009**, *5*, 1016–1026, PMID: 26609610.

(50) Tahir, M. N.; Ren, X. Comparing particle-particle and particle-hole channels of the random phase approximation. *Phys. Rev. B* **2019**, *99*, 195149.

(51) Klimeš, J.; Kaltak, M.; Maggio, E.; Kresse, G. Singles correlation energy contributions in solids. *J. Chem. Phys.* **2015**, *143*, 102816.

(52) Modrzejewski, M.; Yourdkhani, S.; Śmiga, S.; Klimeš, J. Random-Phase Approximation in Many-Body Noncovalent Systems: Methane in a Dodecahedral Water Cage. *Journal of Chemical Theory and Computation* **2021**, *17*, 804–817, PMID: 33445879.

(53) Dunlap, B. I.; Connolly, J. W. D.; Sabin, J. R. On some approximations of Xα method. *J. Chem. Phys* **1979**, *71*, 3396.

(54) Whitten, J. L. Coulomb potential energy integrals and approximations. *J. Chem. Phys.* **1973**, *58*, 4496.

(55) Feyereisen, M.; Fitzgerald, G.; Komornicki, A. Use of approximate integrals in ab initio theory, An application in MP2 energy calculations. *Chem. Phys. Lett.* **1993**, *208*, 359.

(56) Ren, X.; Rinke, P.; Blum, V.; Wieferink, J.; Tkatchenko, A.; Sanfilippo, A.; Reuter, K.; Scheffler, M. *New J. Phys.* **2012**, *14*, 053020.

(57) Levchenko, S. V.; Ren, X.; Wieferink, J.; Johanni, R.; Rinke, P.; Blum, V.; Scheffler, M. Hybrid functionals for large periodic systems in an all-electron, numeric atom-centered basis framework. *Comp. Phys. Comm.* **2015**, *192*, 60.

(58) Lin, P.; Ren, X.; He, L. Accuracy of Localized Resolution of the Identity in Periodic Hybrid Functional Calculations with Numerical Atomic Orbitals. *J. Phys. Chem. Lett.* **2020**, *11*, 3082.

(59) Shang, H.; Carbogno, C.; Rinke, P.; Scheffler, M. Lattice dynamics calculations based on density-functional perturbation theory in real space. *Computer Physics Communications* **2017**, *215*, 26 – 46.

(60) Blum, V.; Hanke, F.; Gehrke, R.; Havu, P.; Havu, V.; Ren, X.; Reuter, K.; Scheffler, M. Ab-initio molecular simulations with numeric atom-centered orbitals. *Comp. Phys. Comm.* **2009**, *180*, 2175.

(61) Havu, V.; Blum, V.; Havu, P.; Scheffler, M. Efficient O(N) integration for all-electron electronic structure calculation using numeric basis functions. *J. Comp. Phys.* **2009**, *228*, 8367.

(62) Ren, X.; Merz, F.; Jiang, H.; Yao, Y.; Rampp, M.; Lederer, H.; Blum, V.; Scheffler, M. All-electron periodic G_0W_0 implementation with numerical atomic orbital basis functions: algorithm and benchmarks. *Phys. Rev. Mater.* **2021**, *5*, 013807.

(63) Fanourgakis, G. S.; Xantheas, S. S. The Flexible, Polarizable, Thole-Type Interaction Potential for Water (TTM2-F) Revisited. *The Journal of Physical Chemistry A* **2006**, *110*, 4100–4106, PMID: 16539435.

(64) Bryantsev, V. S.; Diallo, M. S.; van Duin, A. C. T.; Goddard, W. A. I. Evaluation of B3LYP, X3LYP, and M06-Class Density Functionals for Predicting the Binding Energies of Neutral, Protonated, and Deprotonated Water Clusters. *Journal of Chemical Theory and Computation* **2009**, *5*, 1016–1026, PMID: 26609610.

(65) Kozuch, S.; Gruzman, D.; Martin, J. M. L. DSD-BLYP: A General Purpose Double Hybrid Density Functional Including Spin Component Scaling and Dispersion Correction. *The Journal of Physical Chemistry C* **2010**, *114*, 20801–20808.

(66) Manna, D.; Kesharwani, M. K.; Sylvetsky, N.; Martin, J. M. L. Conventional and Explicitly Correlated ab Initio Benchmark Study on Water Clusters: Revision of the BEGDB and WATER27 Data Sets. *Journal of Chemical Theory and Computation* **2017**, *13*, 3136–3152, PMID: 28530805.

(67) Rakshit, A.; Bandyopadhyay, P.; Heindel, J. P.; Xantheas, S. S. Atlas of putative minima and low-lying energy networks of water clusters n = 3–25. *The Journal of Chemical Physics* **2019**, *151*, 214307.

(68) Burnham, C. J.; Xantheas, S. S. Development of transferable interaction models for water. IV. A flexible, all-atom polarizable potential (TTM2-F) based on geometry dependent charges derived from an ab initio monomer dipole moment surface. *The Journal of Chemical Physics* **2002**, *116*, 5115–5124.

TOC Graphic

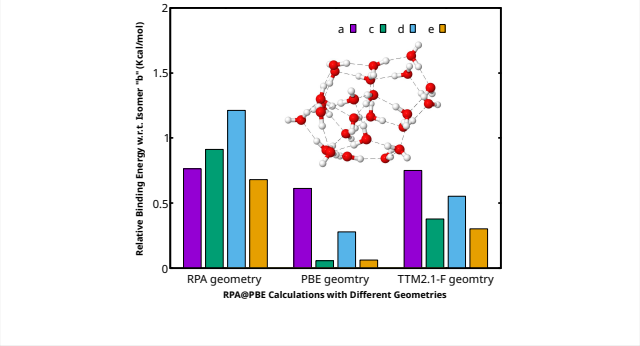
a
c
d
e
Relative Binding Energy w.r.t. Isomer "b" (Kcal/mol)
2
1.5
1
0.5
0
RPA geometry
PBE geomtry
TTM2.1-F geomtry
RPA@PBE Calculations with Different Geometries